



Paleo-denudation rates suggest variations in runoff drove aggradation during last glacial cycle, Crete, Greece

Richard F. Ott¹  | Dirk Scherler^{1,2} | Karl W. Wegmann³ | Mitch K. D'Arcy⁴ | Richard J. Pope⁵ | Susan Ivy-Ochs⁶ | Marcus Christl⁶  | Christoph Vockenhuber⁶ | Tammy M. Rittenour⁷

¹Earth Surface Geochemistry, GFZ German Centre for Geoscience Research, Potsdam, Germany

²Institute of Geological Sciences, Freie Universität Berlin, Berlin, Germany

³Department of Marine, Earth and Atmospheric Sciences & Center for Geospatial Analytics, North Carolina State University, Raleigh, NC, USA

⁴Department of Earth, Ocean and Atmospheric Sciences, University of British Columbia, Vancouver, Canada

⁵School of Environmental Sciences, College of Built and Natural Environment, University of Derby, Derby, UK

⁶Laboratory of Ion Beam Physics, ETH Zürich, Zürich, Switzerland

⁷Geosciences Department, Utah State University, Logan, UT, USA

Correspondence

Richard Ott, GFZ German Centre for Geoscience Research, Telegrafenberg, Potsdam 14473, Germany.
Email: richard.ott@gfz-potsdam.de

Funding information

Swiss National Science Foundation, Grant/Award Number: P2EZP2_191866

Abstract

Fluvial aggradation and incision are often linked to Quaternary climate cycles, but it usually remains unclear whether variations in runoff or sediment supply or both drive channel response to climate variability. Here we quantify sediment supply with paleo-denudation rates and provide geochronological constraints on aggradation and incision from the Sfakia and Elafonisi alluvial-fan sequences in Crete, Greece. We report seven optically stimulated luminescence and ten radiocarbon ages, eight ¹⁰Be and eight ³⁶Cl denudation rates from modern channel and terrace sediments. For five samples, ¹⁰Be and ³⁶Cl were measured on the same sample by measuring ¹⁰Be on chert and ³⁶Cl on calcite. Results indicate relatively steady denudation rates throughout the past 80 kyr, but the aggradation and incision history indicates a link with climate shifts. At the Elafonisi fan, we identify four periods of aggradation coinciding with Marine Isotope Stages (MIS) 2, 4, 5a/b, and likely 6, and three periods of incision coinciding with MIS 1, 3, and likely 5e. At the Sfakia fan, rapid aggradation occurred during MIS 2 and 4, followed by incision during MIS 1. Nearby climate and vegetation records show that MIS 2, 4, and 6 stadials were characterized by cold and dry climates with sparse vegetation, whereas forest cover and more humid conditions prevailed during MIS 1, 3, and 5. Our data thus suggest that past changes in climate had little effect on landscape-wide denudation rates but exerted a strong control on the aggradation–incision behaviour of alluvial channels on Crete. During glacial stages, we attribute aggradation to hillslope sediment release promoted by reduced vegetation cover and decreased runoff; conversely, incision occurred during relatively warm and wet stages due to increased runoff. In this landscape, past hydroclimate variations outcompeted changes in sediment supply as the primary driver of alluvial deposition and incision.

KEYWORDS

alluvial fan, cosmogenic nuclides, fluvial aggradation, incision, paleo-denudation rates, post-burial production, sediment supply

1 | INTRODUCTION

Quaternary glacial cycles are thought to influence sediment production, transport, and deposition, by changing the transport capacity of

streams and the amount of hillslope sediment supplied to them (Bull, 1991). This assumption is based on commonly observed coeval alluvial aggradation and/or incision chronologies that coincide with past climate variations. However, alluvial records respond to changes

This is an open access article under the terms of the [Creative Commons Attribution-NonCommercial](https://creativecommons.org/licenses/by-nc/4.0/) License, which permits use, distribution and reproduction in any medium, provided the original work is properly cited and is not used for commercial purposes.

© 2022 The Authors. *Earth Surface Processes and Landforms* published by John Wiley & Sons Ltd.

in hillslope-to-channel sediment delivery and runoff, and it is challenging to disentangle whether a switch to aggradation or incision is driven by changes in sediment input, water discharge, or both (Scherler et al., 2015). Several Mediterranean studies have reported aggradation of rivers during stadial (cold) stages of the glacial cycle, with one explanation being intensified denudation processes, such as frost cracking, increasing sediment supply (Coltorti & Dramis, 1995; Macklin et al., 2002; Rose et al., 1999; Wegmann & Pazzaglia, 2009). However, paleo-denudation studies on local (e.g. Berger et al., 2008; Shuster et al., 2005; Valla et al., 2012; Vernon et al., 2008) and global scale have produced contradictory results regarding an increase in denudation during glacial climate (Herman et al., 2013; Peizhen et al., 2001; Schildgen et al., 2018; Willenbring & von Blanckenburg, 2010). Linking Quaternary glacial cycles with changes in denudation rates at large scales is complicated by locally variable denudation processes. For example, non-glaciated areas may respond differently to climate change than glaciated regions (Mariotti et al., 2021). Therefore, studying the combined alluvial and denudation response to climate change in controlled settings is an important step towards understanding the controls on aggradation and the impact of climate change on landscapes.

Cosmogenic nuclide concentrations in stream sediment provide a useful tool to quantify hillslope denudation and sediment supply throughout the Quaternary (e.g. Kapannusch et al., 2020; Lenard et al., 2020; Mariotti et al., 2021). Cosmogenic nuclide concentrations from alluvial sediments can be used to calculate paleo-denudation rates, provided concentrations are corrected for nuclide production and decay after sediment deposition (Schaller et al., 2002). These paleo-denudation rates can then be compared with past climate (Mason & Romans, 2018) and aggradation–incision records (Scherler et al., 2015) to study the geomorphic response to climate change. However, most paleo-denudation rate studies measure ^{10}Be in quartz-bearing rocks, creating a knowledge gap regarding the climatic sensitivity of regions with carbonate bedrock.

Several studies have demonstrated that aggradation of alluvial and submarine fans record variations in catchment sediment export in response to Quaternary climate cycles (D'Arcy et al., 2017; Macklin et al., 2002; Pope & Wilkinson, 2005; Waters et al., 2010; Watkins

et al., 2019). However, linking these variations to sediment supply has proven difficult as it remains unclear if denudation in fluvial landscapes increased during a colder climate due to enhanced physical erosion (Hales & Roering, 2007; Marshall et al., 2021). In temperate climates, Marshall et al. (2015) showed a 2.5-fold increase in denudation during stadial intervals using cosmogenic nuclides, whereas other studies do not detect significant variations in denudation over the Pleistocene (Cyr & Granger, 2008; Kapannusch et al., 2020; Schaller et al., 2002). In the southwestern United States, Pleistocene paleo-denudation rates show only minor variations across orbitally driven hydroclimate cycles (Mason & Romans, 2018), despite major concurrent variations in catchment sediment flux (D'Arcy et al., 2017). As short source-to-sink systems, alluvial fans respond rapidly to changing climatic conditions. When coupled with paleo-denudation rate measurements, alluvial fans are ideal for investigating how climate changes affect hillslope sediment supply to channels, and how such variations in supply are transferred into the sedimentary record (Savi et al., 2014).

To investigate the response of hillslope denudation and stream aggradation–incision behaviour to climate variations in a fluvial landscape, we studied Late Pleistocene deposits of the Sfakia and Elafonisi fan complexes in western Crete, Greece (Figure 1). We take advantage of geochronologic ages published for the Sfakia fan (Pope et al., 2008, 2016) and contribute new geomorphic mapping results along with luminescence and radiocarbon dating for the Elafonisi fan system. In addition to studying changes in hillslope denudation, we measured cosmogenic ^{10}Be and ^{36}Cl in quartz-bearing and limestone lithologies, respectively, from modern and Late Pleistocene sediment. Together, these data allow us to compare variations in aggradation and incision with concurrent hillslope denudation rates and investigate the sensitivity of the sedimentary record to variations in runoff and sediment supply.

2 | BACKGROUND

Crete occupies a forearc high within the Hellenic Subduction Zone, where the African Plate subducts beneath the Aegean Plate at a rate

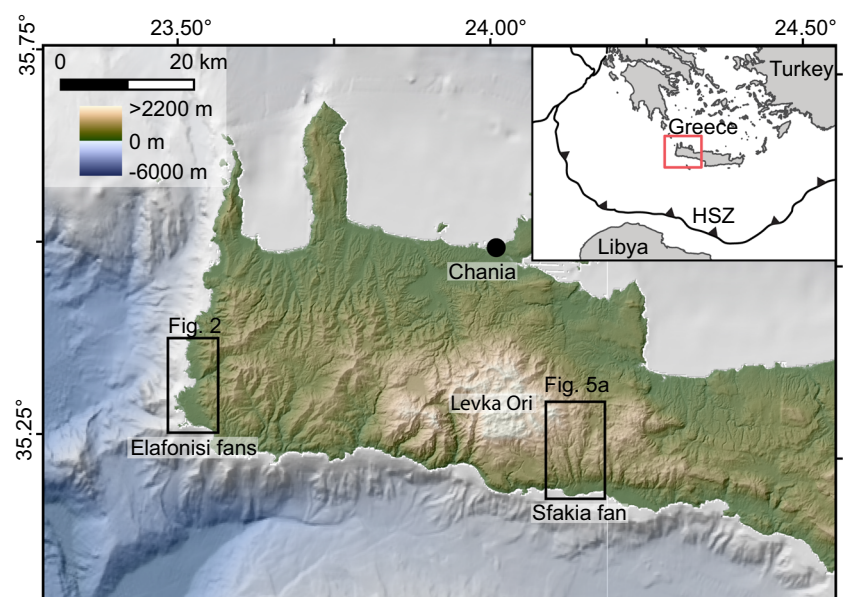


FIGURE 1 Overview of the study sites in western Crete, Greece. Inset: Location of western Crete within the Hellenic subduction zone (HSZ). [Color figure can be viewed at [wileyonlinelibrary.com](https://onlinelibrary.wiley.com)]

of ~ 35 mm/a (Reilinger et al., 2006, 2010). Most of Crete is part of a nappe pile stacked during mid-Cenozoic subduction and exhumed during subsequent extensional deformation in the late Cenozoic (Fassoulas et al., 1994; Jolivet & Brun, 2010). The Sfakia fan is a large (~ 3.2 km²) telescopic fan and the westernmost of seven coalesced fans (Nemec & Postma, 1993). The 24 km² catchment sourcing the Sfakia fan consists mostly of platy limestones with interbedded cherts of the Jurassic to Eocene Plattenkalk Formation and limestone of the Jurassic Trypali unit (Creutzberg et al., 1977). The Elafonisi fan system consists of eight adjacent alluvial fans along the southwestern coast of Crete. We collected samples along the Stomio River, which drains the largest (35 km²) catchment of the Elafonisi area and has several river terraces preserved near its outlet. Additionally, we sampled two ~ 1.5 km² catchments with telescopic fans near Livadia and Chrissoskalitissa (Figure 2). The Stomio and Livadia catchments are dominated by the Carboniferous to Middle Triassic Phyllite-Quartzite (PQ) unit, whereas the Plattenkalk Formation is exposed in the Chrissoskalitissa catchment.

The Elafonisi and Sfakia fans are situated at the coast and are sensitive to base-level changes in response to eustatic sea-level change and vertical crustal motion. Ott et al. (2019b) documented average uplift rates of ~ 1.2 mm/a since 71 ka at Elafonisi and < 0.1 mm/a since 125 ka for the hanging wall of the Sfakia fault on which the fan is deposited. The Krios paleoshoreline, which can be traced along the western coast of Crete, documents Late Holocene uplift during either a single (Shaw et al., 2008) or a sequence of earthquakes (Ott et al., 2021) by about 8 m at Elafonisi and 2.9 m at Sfakia (Angelier, 1979; Ott et al., 2021). However, on a Late-Pleistocene timescale, rock uplift rates along the coast of Crete are relatively steady (Gallen et al., 2014; Ott et al., 2019b; Robertson et al., 2019; Strasser et al., 2011).

In contrast to the Elafonisi fans, the Sfakia fan has been studied in detail for its sedimentology and depositional history. Two main units can be distinguished (Nemec & Postma, 1993; Pope et al., 2008, 2016), which we refer to as Quaternary deposit 1 (Qt1) and Qt2. Qt1 is only preserved at the head of the Sfakia fan and is dominated by thick beds of subangular to subrounded, cobble-to-boulder-sized clasts, interpreted as debris-flow deposits (Nemec & Postma, 1993; Pope et al., 2008). Unit Qt2 is inset into Qt1 and consists of better-sorted, pebble-to-cobble streamflow deposits with interspersed debris-flow layers. Both fan units contain layers of fine-grained red silt with angular pebbles and pale tan silt lenses, representing paleosols and small aeolian dune deposits, respectively (Nemec & Postma, 1993). For a more detailed description of the sedimentology of the Sfakia fan, we refer the reader to Nemec and Postma (1993) and Pope et al. (2008). Based on published geochronologic ages, Qt1 was deposited mainly during MIS 5, and after a brief period of incision at the beginning of MIS 4, Qt2 was deposited from MIS 4 to 2 (Pope et al., 2008, 2016). Qt2 is now deeply incised; based on archaeological evidence, the incision must have started before about 5.5 ka (Pope et al., 2008).

Today, both catchments are dominated by a hot-summer Mediterranean climate (Csa in the Köppen-Geiger climate classification) (Beck et al., 2018). The mean annual precipitation for the Elafonisi and Sfakia catchments is 817 and 656 mm/a, respectively. The lower precipitation rate and reduced water-holding capacity of the limestone terrain dominating the Sfakia catchment likely explains its

lower vegetation density compared to the Elafonisi area (Ott, 2020). Eastern Mediterranean climate during the last glacial cycle was characterized by cold and dry stadials (MIS 2, 4, 6) and comparatively warm and wet interglacials and interstadials (MIS 1, 3, 5) (Cheddadi & Rossignol-Strick, 1995; Langgut et al., 2011). A potential glaciation of the Levka Ori Mountains above the Sfakia catchment remains debated (Hughes & Woodward, 2017). Nevertheless, even if small glaciers existed in the Levka Ori Mountains, the Sfakia catchment presently lacks surficial streams connecting the fan to the highest areas of the Levka Ori. A potential hydrologic connection to the high-altitude glaciated areas may have existed, but due to the small extent of the potentially glaciated area compared to the catchment size (24 km²), we assume no major glacial influence on the Sfakia fan.

Catchment-wide denudation rates on Crete have been determined from catchments draining the PQ bedrock unit in western Crete and carbonate catchments throughout the island (Ott et al., 2019a). ¹⁰Be-derived denudation rates in western Crete are around 0.11 mm/a, and ³⁶Cl-derived denudation rates from carbonate areas average 0.13 mm/a (Ott et al., 2019a). Ott et al. (2019a) concluded that the carbonate massifs and PQ cored mountains in western Crete denude at similar rates but that infiltration of precipitation into the karst system permits the carbonate mountains to form steeper topography despite experiencing similar uplift rates.

3 | MATERIALS AND METHODS

We built on the existing geochronological framework established by 39 luminescence and U-Th ages from the Sfakia fan (Pope et al., 2008, 2016) and collected samples for paleo-denudation rates from dated and rapidly buried layers. For the previously undated Elafonisi fan system, we established the geochronology using luminescence and radiocarbon dating. Samples for paleo-denudation rates were taken from sedimentary layers with age control, and either ³⁶Cl calcite or ¹⁰Be quartz concentrations were measured, depending on the sediment source.

3.1 | Field mapping and digital elevation data

The redness of soil B-horizons in arid landscapes is related to the concentration of secondary iron oxides and has been used extensively for relative age determination of alluvial fan surfaces (Ferrier & Pope, 2012; Harvey et al., 1999). The redness of B-horizons within soils was determined using a Munsell colour chart on the fine-grained matrix between clasts. Mapping of the Quaternary (Qt) units is based on soil redness, geomorphic position (elevation), observed unconformities, and abrupt changes in fan surface slope. At the Sfakia fan, we used a drone for aerial images and built a digital elevation model (DEM) using photogrammetric software (Agisoft). At Elafonisi, a 5 m DEM was provided by the Hellenic Cadastre SA. For mapping marine paleoshorelines, the inner shoreline angle (ISA) was estimated in the field, and its elevation was measured with a laser range finder. ISA refers to the intersection point between the marine abrasion platform and the paleo-sea cliff and approximates the paleo-sea level during paleoshoreline formation (Lajoie, 1986).

3.2 | Optically stimulated luminescence

We collected seven samples from fan and river-terrace deposits within the Elafonisi study area to constrain the timing of sediment deposition and burial by optically stimulated luminescence (OSL) measurements (Table 1). Samples were collected in light-proof metal cylinders driven 0.25 m horizontally into sand-dominated sedimentary lenses. In addition, moisture samples were collected in airtight film canisters from the sample cylinder location, and environmental dose rate samples were collected from sediment within an ~30 cm radius surrounding the OSL sample.

OSL samples were analysed by single-aliquot regenerative dose (SAR) procedures for dating quartz sand (Murray & Wintle, 2000; Wintle & Murray, 2006) at the Utah State University Luminescence Laboratory, Logan, UT, USA. Samples were processed under safelight conditions using sieving, gravity separation, and acid treatments with HCl and HF to isolate the quartz component of the 90–150 μm grain size range following procedures outlined by Aitken (1998) and described in Rittenour et al. (2003, 2005). Samples were analysed on Risø OSL/TL DA-20 luminescence readers with blue/green (470 nm, 36 W/m²) stimulation and detection through 7.5-mm UV filters (U-340). Stimulation was conducted at 125°C following 240°C preheats (10 s) for regenerative and natural doses. Dose–response curves were created using five sensitivity-corrected regenerative dose points (including a repeat and zero-dose step). The resultant data were fit with a saturating exponential curve from which the equivalent dose

(D_E ; reported in Figure S1) is determined. The D_E , reported in Table 1, is based on a central age model (Galbraith & Roberts, 2012) from the measurement of at least 20 aliquots of sand mounted on a 2 mm-diameter area of the measurement disks (~200 grains/aliquot). Dose rate measurements were determined by chemical analysis of the U, Th, K, and Rb content using ICP-MS and ICP-AES techniques and conversion factors (Guérin et al., 2011) (Table S4). The contribution of cosmic radiation to the dose rate was calculated using sample depth, elevation, and latitude/longitude following Prescott and Hutton (1994). Sediments were dry when collected, but a value of 3 ± 3 wt% water content was considered representative of their burial history. Total dose rates were calculated based on water content, radioisotope concentration, and cosmic contribution (Adamiec & Aitken, 1998; Aitken, 1998) (Table S4).

3.3 | Radiocarbon dating

To constrain the end of the last depositional phase at the Sfakia fan, we dated carbonate rinds (thickness 1–5 mm) from the upper metre of a coastal cliff at the distal end of the Sfakia fan (Table 2). The dating of carbonate cement has been utilized in similar studies to constrain the timing of cementation periods, thereby providing a minimum depositional age (Geyh & Eitel, 1997; Giresse & Martzluft, 2015). All samples were leached with 0.5 M HCl to remove possible surface contamination, put in 12 ml septum-sealed vials (Labco), flushed with

TABLE 1 Luminescence age information from the Elafonisi fan area

| Sample | Lab-ID | Grain size (μm) | No. aliquots [†] | Dose rate [‡] (Gy/kyr) | Equivalent dose (D_E) [§] $\pm 2\sigma$ (Gy) | OSL age $\pm 1\sigma$ (ka) |
|---------------|---------|------------------------------|---------------------------|---------------------------------|---|----------------------------|
| KWW-102508-5 | USU-485 | 90–150 | 23 (50) | 1.42 \pm 0.07 | 81.97 \pm 9.31 | 57.81 \pm 5.90 |
| KWW-102408-1A | USU-486 | 90–150 | 29 (57) | 0.73 \pm 0.04 | 17.28 \pm 2.53 | 23.74 \pm 2.73 |
| KWW-102408-1D | USU-487 | 75–150 | 36 (49) | 0.97 \pm 0.05 | 14.38 \pm 1.66 | 14.75 \pm 1.53 |
| KWW-102408-2 | USU-488 | 90–150 | 24 (55) | 1.72 \pm 0.08 | 138.16 \pm 15.39 | 80.29 \pm 8.05 |
| KWW-102508-2 | USU-489 | 75–150 | 28 (57) | 1.54 \pm 0.07 | 87.37 \pm 9.73 | 56.81 \pm 7.88 |
| KWW-102508-2 | USU-490 | 63–125 | 26 (69) | 1.89 \pm 0.08 | 96.36 \pm 12.49 | 50.92 \pm 7.82 |
| 062009-1 | USU-600 | 75–150 | 31 (60) | 1.83 \pm 0.08 | 112.80 \pm 11.12 | 61.67 \pm 5.98 |

[†]Age analysis using the single-aliquot regenerative dose procedure of Murray and Wintle (2000) on small, 2–5 mm aliquots of quartz sand. The number of aliquots used in age calculation and the number of aliquots analysed are in parentheses.

[‡]Assumed $3.0 \pm 3.0\%$ as moisture content over burial history.

[§]Equivalent dose (D_E) calculated using the Central Age Model (CAM) of Galbraith and Roberts (2012).

TABLE 2 Radiocarbon data from the Sfakia and Elafonisi fans

| Sample | Lab-ID | Lat (°) | Long (°) | $\delta^{13}\text{C}$ | ¹⁴ C age BP | calBP (2 σ) | Dated material |
|--------|--------------|----------|----------|-----------------------|------------------------|---------------------|-------------------------|
| 1A | 105011.1.1 | 35.19327 | 24.15583 | –12.69 | 4699 \pm 78 | 5593–5290 | carbonate rind |
| 1B | 105012.1.1 | 35.19327 | 24.15583 | –10.10 | 5235 \pm 74 | 6266–5765 | carbonate rind |
| 1C | 105013.1.1 | 35.19327 | 24.15583 | –8.75 | 8486 \pm 82 | 9658–9283 | carbonate rind |
| 1D | 105014.1.1 | 35.19327 | 24.15583 | –13.35 | 9475 \pm 87 | 11 107–10 507 | carbonate rind |
| 2A | 105015.1.1 | 35.19327 | 24.15583 | –20.12 | 3960 \pm 72 | 4786–4155 | carbonate rind |
| 2B | 105016.1.1 | 35.19327 | 24.15583 | –15.44 | 4018 \pm 76 | 4816–4254 | carbonate rind |
| 2C | 105017.1.1 | 35.19327 | 24.15583 | –14.79 | 6351 \pm 79 | 7428–7027 | carbonate rind |
| 2D | 105018.1.1 | 35.19327 | 24.15583 | –17.07 | 3575 \pm 73 | 4086–3650 | carbonate rind |
| 2E | 105019.1.1 | 35.19327 | 24.15583 | –6.59 | 5590 \pm 77 | 6558–6214 | carbonate rind |
| 3 | UCIAMS-68078 | 35.30571 | 23.54750 | –7.5 | 9910 \pm 20 | 11 394–11 243 | terrestrial snail shell |

helium, dissolved with H₃PO₄ (85%), and converted to graphite targets using automated graphitization equipment (Synal et al., 2007). Accelerator mass spectrometry (AMS) was carried out at the Laboratory for IonBeam Physics at ETH Zürich using a Mini Carbon Dating System (MICADAS) AMS (Synal et al., 2007). Oxalic acid II NIST standard was used for fractionation correction and standard normalization. Radiocarbon ages were converted to calendar years with IntCal 20 (Reimer et al., 2020).

Additionally, we dated a terrestrial gastropod (snail) shell sampled from a silt layer contained within a channel incised into the fan surface at the Chrissoskalitissa site to constrain the timing of fan-surface abandonment and the onset of incision (Table 1, Figure 3G). After sieving bulk sediment and microscopic examination, a single, intact shell was selected. The shell was broken and cleaned in milli-Q water with sonic vibration before removing the outer surfaces with dilute HCl. This sample was analysed at the University of California Irvine Keck Carbon Cycle AMS Facility (UCIAMS), following standard cleaning and preparation techniques. The reported radiocarbon age was corrected for isotopic fractionation according to Stuiver and Polach (1977), and sample preparation backgrounds were subtracted based on measurements of ¹⁴C-free calcite. The sample $\delta^{13}\text{C}$ value was measured relative to standards traceable to Pee Dee Belemnite, using a Thermo Finnigan Delta Plus stable isotope ratio mass spectrometer with gas bench input.

3.4 | Cosmogenic nuclide measurements

We analysed 11 cosmogenic nuclide samples to determine (paleo-) denudation rates. For three samples sourced by the quartz-rich PQ

unit (Stomio River and Livadia at Elafonisi), we measured only ¹⁰Be on quartz (Table 3). In the Plattenkalk-sourced carbonate sediments from the Chrissoskalitissa fan, we measured only ³⁶Cl concentrations on calcite. For five samples from the Sfakia fan, we measured ³⁶Cl concentrations on calcite and ¹⁰Be on chert to test if denudation rates from both nuclides agree. To compare Holocene denudation rates with rates of paleo-denudation during the Late Pleistocene, we also measured cosmogenic nuclide concentrations in modern stream sediment. At the Elafonisi site, a ¹⁰Be concentration from modern sediments in the Stomio River was published by Ott et al. (2019a) (location in Figure 2).

3.4.1 | ³⁶Cl measurements

We collected sediment samples with grain sizes between 1 and 4 mm, for consistency with ³⁶Cl catchment-wide denudation rate measurements by Ott et al. (2019a). The samples were crushed to <1 mm with a disc mill, after which we separated the fraction for ¹⁰Be measurement on chert from the Sfakia fan samples. Meteoric ³⁶Cl was removed by repeated etching with 2 M HNO₃ and rinsing with milli-Q water. A ³⁵Cl spike (Ivy-Ochs et al., 2004) was added to the samples before their dissolution with HNO₃ (Prager et al., 2009). The samples were measured at the 6MV TANDEM AMS at ETH Zürich, which utilizes a gas-filled magnet to separate the ³⁶S isobar (Vockenhuber et al., 2019). They were calibrated using the internal K382/4 N standard (Christl et al., 2013) (Table 3). The chemical composition of the ³⁶Cl samples was determined with an ICP-MS for both the bulk sample and the undissolved remnants to determine the composition of the bulk sample and the dissolved target mineral. The compositional data for bulk rock and target minerals are reported in Table S1.

TABLE 3 ¹⁰Be and ³⁶Cl AMS results

| Sample | AMS code | Lat (°) | Long (°) | Elevation (m) | ¹⁰ Be/ ⁹ Be | Error (%) | Carrier (mg) | Weight (g) | ¹⁰ Be (at/g) | |
|------------------------|----------|----------|----------|---------------|------------------------------------|-----------|--------------|------------|-------------------------|------------------|
| ¹⁰Be | | | | | | | | | | |
| EI-919-1 | ZB7493 | 35.33412 | 23.56767 | 96 | 3.23E-14 | 9.3% | 0.2456 | 13.72 | 34 200 ± 5000 | |
| EI-919-2 | ZB7494 | 35.32846 | 23.55132 | 34 | 3.84E-14 | 6.9% | 0.2507 | 16.37 | 35 500 ± 4000 | |
| EI-617-PE-4 | TB3908 | 35.35393 | 23.53772 | 48 | 4.22E-14 | 8.7% | 0.247 | 35.33 | 15 600 ± 2400 | |
| SF-919-1 [†] | s16955 | 35.21184 | 24.15585 | 220 | 1.05E-13 | 5.28 | 0.161 | 44.75 | 24 353 ± 1441 | |
| SF-919-11 [†] | s16956 | 35.19444 | 24.15918 | 18 | 1.13E-13 | 4.93 | 0.163 | 33.26 | 35 787 ± 1972 | |
| SF-919-12 [†] | s16957 | 35.19665 | 24.15364 | 67 | 1.41E-13 | 4.82 | 0.146 | 48.48 | 27 667 ± 1444 | |
| SF-919-14 [†] | s16958 | 35.19306 | 24.15426 | 24 | 3.41E-13 | 3.93 | 0.163 | 60.64 | 60 546 ± 2439 | |
| SF-919-15 [†] | s16959 | 35.19306 | 24.15426 | 24 | 1.33E-13 | 5.23 | 0.138 | 44.03 | 27 158 ± 1537 | |
| Sample | AMS code | Lat (°) | Long (°) | Elevation (m) | ³⁶ Cl/ ³⁵ Cl | Error (%) | Carrier (mg) | Weight (g) | ³⁶ Cl (at/g) | |
| ³⁶Cl | | | | | | | | | | |
| EI-919-3 | CV3829 | 35.30663 | 23.55487 | 174 | 2.31E-14 | 10.11 | 236.3 ± 1.6 | 3.653 | 63.36 | 76 000 ± 12 317 |
| EI-919-4 | CV3830 | 35.30588 | 23.54728 | 96 | 3.07E-14 | 7.45 | 312.2 ± 1.8 | 3.692 | 67.95 | 131 000 ± 14 876 |
| EI-919-5 | CV3831 | 35.30588 | 23.54728 | 106 | 2.37E-14 | 8.63 | 299.8 ± 2.1 | 3.658 | 66.06 | 93 000 ± 13 546 |
| SF-919-1 | CV3832 | 35.21184 | 24.15585 | 220 | 1.12E-13 | 5.67 | 23 ± 2.3 | 3.668 | 41.62 | 195 000 ± 12 030 |
| SF-919-11 | CV3833 | 35.19444 | 24.15918 | 18 | 1.26E-13 | 5.04 | 18.1 ± 2 | 3.666 | 43.30 | 205 000 ± 11 195 |
| SF-919-12 | CV3834 | 35.19665 | 24.15364 | 67 | 1.17E-13 | 5.22 | 15.8 ± 2 | 3.671 | 39.50 | 202 000 ± 11 496 |
| SF-919-14 | CV3835 | 35.19306 | 24.15426 | 24 | 1.07E-13 | 5.62 | 25.7 ± 29.1 | 3.673 | 24.37 | 298 000 ± 18 343 |
| SF-919-15 | CV3836 | 35.19306 | 24.15426 | 24 | 1.14E-13 | 4.91 | 18 ± 0.9 | 3.675 | 42.66 | 187 000 ± 10 097 |

Average blank ratios for corrections ¹⁰Be (Cologne) 3.4E-15 ± 2.3E-15, ¹⁰Be (Zürich) 7.2E-15 ± 8.2E-16, ³⁶Cl 4.5E-15 ± 1.9E-15.

[†]Measured at Cologne AMS.

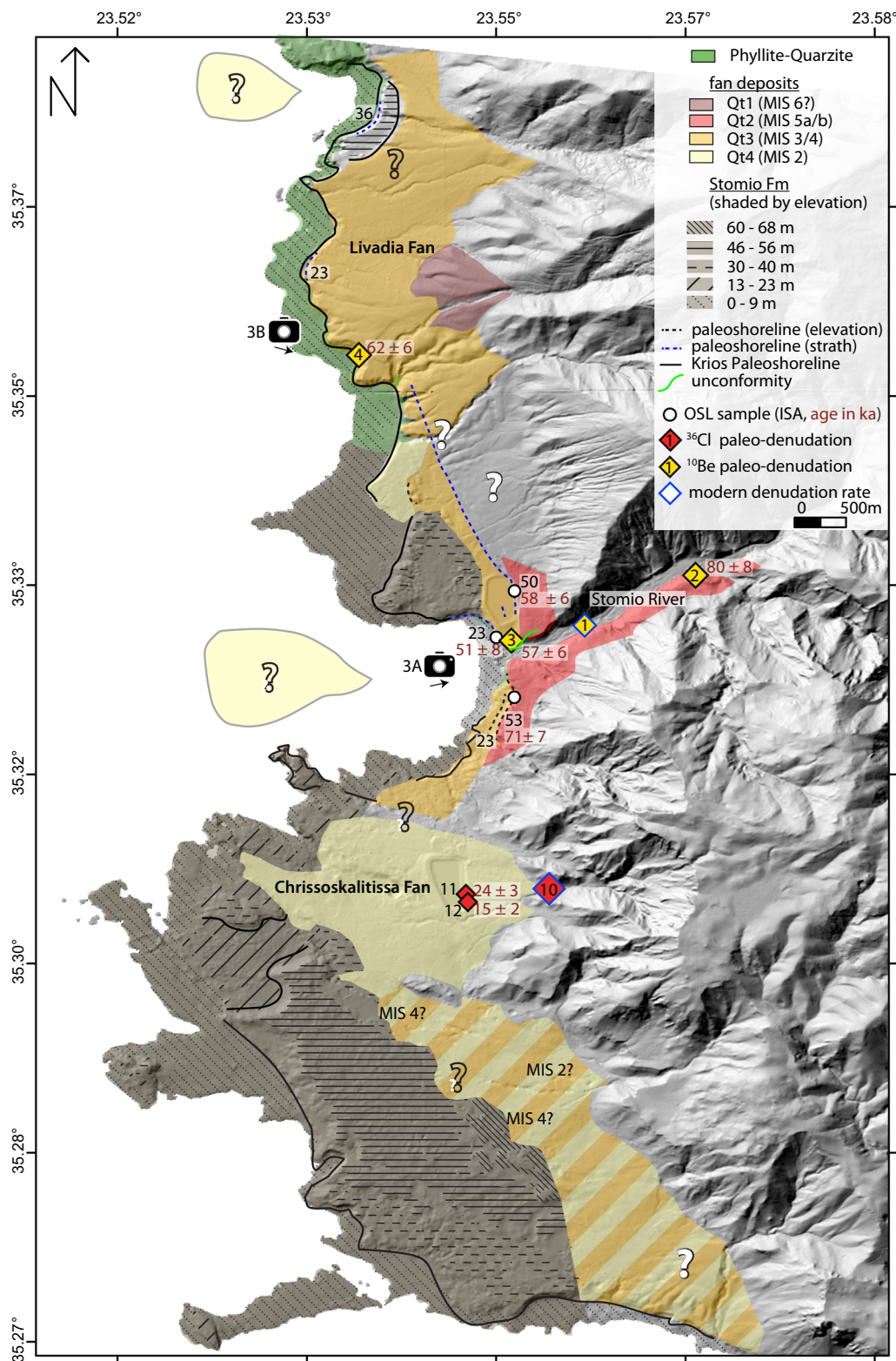


FIGURE 2 Elafonisi mapping results and geochronology. Numbers for denudation rate samples correspond to Table 4. In addition, for paleoshorelines, the elevation of the inner shoreline angle (ISA) is indicated. [Color figure can be viewed at [wileyonlinelibrary.com](https://onlinelibrary.wiley.com/doi/10.1002/esp.3492)]

3.4.2 | ^{10}Be measurements

In the northern Elafonisi area, we collected three samples of sand and processed the 0.25–0.71 mm size fraction for ^{10}Be analysis. We separated quartz from other minerals by magnetic separation and repeated etching with hydrochloric, hydrofluorosilicic, and hydrofluoric acid. A ^9Be carrier was added, and beryllium was extracted using ion

chromatography (Bierman et al., 2002). The $^{10}\text{Be}/^9\text{Be}$ isotope ratios were measured by the 500 kV TANDY accelerator mass spectrometer at ETH Zürich and calibrated using the S2007 N ^{10}Be standard (Christl et al., 2013) (Table 3). The five chert samples from the Sfakia fan were cleaned by etching with hydrochloric and nitric acid and measured at the Cologne AMS facility (Dewald et al., 2013) relative to standards KN01-6-2 and KN01-5-3.

3.5 | Post-burial production and (paleo-) denudation rate calculations

We calculated (paleo-)denudation rates with the CRONUScalc v2.1 tools (Marrero et al., 2016a). However, we modified the scaling factor functions (scalefacs1026, scalefacs36) to calculate scaling factors based on a pixel-by-pixel approach for the entire catchment area. Catchment scaling factors were calculated on a 30-m SRTM DEM for modern and paleo-denudation rates. Time-dependent production

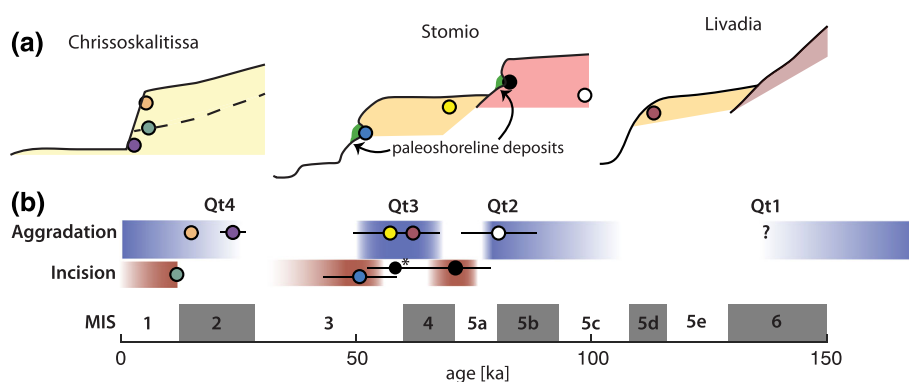
rates were calculated with the Stone (2000) scaling and accounting for geomagnetic variations after Nishiizumi et al. (1989). We assume a bulk density of 2.65 and 2.2 g/cm³ for the bedrock and fan deposits (Rodés et al., 2011), respectively, with an uncertainty of 0.1 g/cm³.

We developed a Monte Carlo routine that utilizes the CRONUScalc v2.1 production rate functions to estimate post-burial production ('PostPro') (Ott, 2022). First, the age of the sampled layer and age constraints on layers above are used to build a time-depth history, assuming that aggradation between two layers of known age



FIGURE 3 Field pictures from Elafonisi fan system. See Figure 2 for image locations. (a) View of the Stomio River mouth. The 23 m paleobeach strath and deposit are highlighted in yellow for visibility. (b) View of the Livadia fan. (c) Marine deposit of the Stomio Formation containing cobbles, pebbles, and algal constructions. (d) Close-up of unit Qt3. (e) Paleobeach deposited on strath in gypsum bedrock. (f) Dated channel in Qt2 deposit. (g) Dated section of the Chrissoskalitissa fan. The white circles are OSL samples; the yellow circle is a radiocarbon sample of a fill deposit inset into the Qt4 fan. [Color figure can be viewed at [wileyonlinelibrary.com](https://onlinelibrary.wiley.com)]

FIGURE 4 (a) Conceptual sketch of relative sample position for the Chrissoskalitissa, Stomio, and Livadia sites. The dots correspond to sampling locations, and the colours match the ages in (b). (b) Elafonisi aggradation (blue) and incision (red) constraints versus marine isotope stadial and interstadial extents since 150 ka. The asterisk (*) indicates an OSL sample age from a paleoshoreline excluded from the geochronologic interpretation (see text). [Color figure can be viewed at [wileyonlinelibrary.com](https://onlinelibrary.wiley.com)]



occurred at a constant rate. Then, for each paleo-denudation sample, we generated 5000 synthetic time–depth histories by randomly drawing an age and depth for each dated layer, assuming normally distributed ages and depths defined by the geochronologic ages, measured depths, and their respective uncertainties. In addition, for every simulation, production rates are drawn from normal distributions with uncertainties of 8% in ^{10}Be spallation production (Phillips et al., 2016), 30% in muon production (three times the value of Phillips et al., 2016 to avoid underestimation of the uncertainty), and ^{36}Cl production rate uncertainties based on Marrero et al. (2016b) (for spallation and muon production we use the average of the relative uncertainties in the dominating Ca and K production). Subsequently, post-depositional production and decay are computed for every synthetic burial history. The mean post-depositional nuclide concentration from the sampled layer is then subtracted from the measured concentration, and the uncertainty in post-burial production is propagated together with the AMS and blank correction uncertainty. A link to the PostPro code is provided in the [Data Availability statement](#) with example input from this study.

The computation of post-burial production requires an age for the end of deposition above the sample. In most sampled locations, we used the mean age of the youngest deposited layer and the oldest incision constraint, which often corresponds to the depositional age of the next younger unit. However, at the Sfakia fan and a Stomio River terrace (Elafonisi), we also report an alternative scenario based on less conservative assumptions of surface abandonment. The analysis presented in the main text is based on the more conservative estimates for surface abandonment ages listed in Table 4. We report a detailed description of constraints on surface abandonment and uncertainty calculation in Table S2. Table S3 documents the results for the alternative burial scenario.

4 | RESULTS

4.1 | Elafonisi fan

4.1.1 | Depositional chronology

At the Elafonisi fan system, four units of Quaternary deposits (Qt) can be identified (Figure 2). These units are bounded by erosional unconformities and inset into each other. Qt1 consists of a steep (10°), cobble-dominated fan in the highest geomorphic position on the Livadia fan (Figure 2). The high soil redness (2.5YR 4/8 to 2.5YR 3/6, red to dark red), the elevated geomorphic position, and the deep incision of Qt1

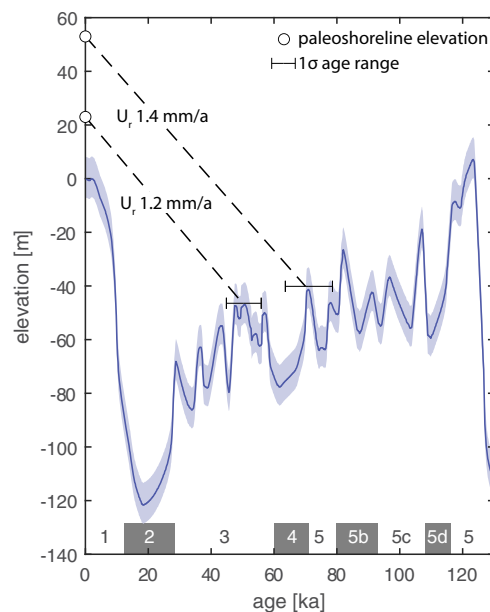


FIGURE 5 Sea-level correlation for the two dated paleoshorelines at the Elafonisi area using the eustatic curve of Lambeck and Chappell (2001). Dashed lines indicate the rock uplift rates based on sea-level highstand correlations. Marine isotope stages are highlighted along the x-axis. [Color figure can be viewed at [wileyonlinelibrary.com](https://onlinelibrary.wiley.com)]

suggest a relatively old formation age (Figure 3b). Unit Qt2 is deposited along the Stomio River and its outlet (Figure 2). Qt2 forms a continuous river terrace 60–70 m above the stream (Figure 3a) of well-cemented, poorly to moderately well-sorted fluvial sediments of sand to boulder size (Figure 3f). Qt3 is inset into Qt2 at the mouth of the Stomio River (Figures 3a and 4a) and Qt1 at the Livadia fan (Figures 3b and 4a). At the Livadia fan, Qt3 is characterized by cobble-dominated, poorly sorted fan deposits of red soil colour (2.5YR 4/8), with some thinly (~ 10 cm) bedded silt to sand-sized lenses. Closer to the mouth of the Stomio River, Qt3 is strongly cemented and consists of coarser grains ranging from sands to boulders (Figure 3d). The gradient of the Qt3 fan surface (6°) is substantially lower than the Qt1 fan surface. Qt4 is inset into the Qt3 fan at the Livadia fan and exhibits similar sedimentology but significantly lower soil redness (2.5YR 6/4; light reddish-brown). At the Chrissoskalitissa fan, a water reservoir is cut into a Qt4 fan surface and exposes ~ 20 m of weakly bedded, poorly cemented sand to cobble-sized clasts (Figure 3g) with similarly low soil redness. Across all Qt units, the average grain size appears greatest along the Stomio River and its outlet. Strong cementation of units along the Stomio River deposits points to an admixture of the Plattenkalk unit's carbonates.

All mapped Qt units are currently being incised. Their cross-cutting stratigraphic relationships and differences in soil redness confirm a relative sequence of events starting with deposition of Qt1 and ending with Qt4, with periods of incision separating aggradation intervals.

Several paleoshoreline levels are cut into the bedrock and Qt units, documenting long-term rock uplift. Four paleoshoreline deposits were identified, with inner shoreline angles (ISA), the intersection between the marine abrasion platform and the paleoclipf, ranging in elevation from 8 to 53 m (Figure 2). These deposits are found on bedrock straths (Figure 3e) or erosional surfaces and along cliffs within the Qt deposits. In addition, marine deposits crop out near the coastline (Figure 2) and have previously been assigned a Miocene to Pliocene age (Mountrakis et al., 2013), albeit with poor age control. This marine formation consists of unsorted cobbles, pebbles, and sand derived from the PQ unit, mixed with algal constructions in a matrix-dominated, well-cemented carbonate rock (Figure 3c). We interpret these deposits as the subaqueous part of the Stomio River delta system that has been uplifted above sea level and refer to this unit as the Stomio Formation.

New chronological constraints

Our seven luminescence ages range from approximately 81 to 15 ka and show a younging trend with lower (inset) topo-geomorphic positions (Table 1, Figure 4), which agrees with the relative sequence of events established by field observations. A 15-m-wide channel cross-section from ~20 m below the top of the Qt2 deposit (Figure 3f) was dated to 80 ± 8 ka. At the Livadia fan, a sample 10 m below the Qt3 fan surface returned an age of 62 ± 6 ka. Near the mouth of the Stomio River, Qt3 was dated to 57 ± 8 ka, 3 m below the deposit surface. Aggradation of the Qt4 Chrissoskalitissa fan is constrained by the age of 24 ± 3 ka near the bottom, and 15 ± 2 ka, 3 m below the fan surface. The switch from aggradation to subsequent incision at Chrissoskalitissa is constrained by a radiocarbon age from a snail shell within the channel that incised the fan at 11.3–11.2 ka (2σ range)

(Figure 3g). Two paleoshorelines near the Stomio River mouth, with ISAs of 53 and 23 m, were dated to 58 ± 6 and 51 ± 8 ka, respectively.

Synthesis of new and published chronological data

Our new geochronologic ages and published observations constrain the timing of aggradation and incision at Elafonisi (Figure 4). Our luminescence age of Qt2 suggests deposition around MIS 5a/b. A paleoshoreline forming a paleoclipf in Qt2 south of the Stomio River mouth was dated to 71 ± 7 ka (Ott et al., 2019b) and potentially marked the incision into Qt2. However, we dated a paleoshoreline at the same elevation to 58 ± 6 ka north of the Stomio River mouth. Both ages overlap within uncertainty, yet paleoshorelines on Crete have been shown to form during sea-level highstands and record relatively steady uplift rates (Gallen et al., 2014; Ott et al., 2019b; Robertson et al., 2019). Therefore, we assume the 71 ± 7 ka age lies closer to the true age because it matches the MIS 5a highstand, the most commonly preserved highstand on Crete (Ott et al., 2019b), and infer an uplift rate almost identical to the one derived from the paleoshoreline below (see Section 4.1.2). We note that the 58 ± 6 ka sample was collected at a shallow depth below the surface soil and younger grains may have been worked into the sediment from bioturbation (see Figure S1, sample USU-485). A paleoshoreline dated to 51 ± 8 ka and inset against Qt3 serves as a minimum age constraint for the end of Qt3 aggradation, which occurred around 57–62 ka. Aggradation of Qt4 occurred during MIS 2 based on our two luminescence ages from Chrissoskalitissa, and incision of Qt4 commenced about 11 ka.

4.1.2 | Uplift rates

We dated two uplifted paleoshorelines at the Elafonisi site. The correlation of the paleoshorelines with eustatic sea-level highstands (Lambeck & Chappell, 2001) allows for calculating time-averaged uplift rates of 1.2 and 1.4 mm/a (Figure 5). The five different marine abrasion platforms cut into the Stomio Formation also exemplify long-

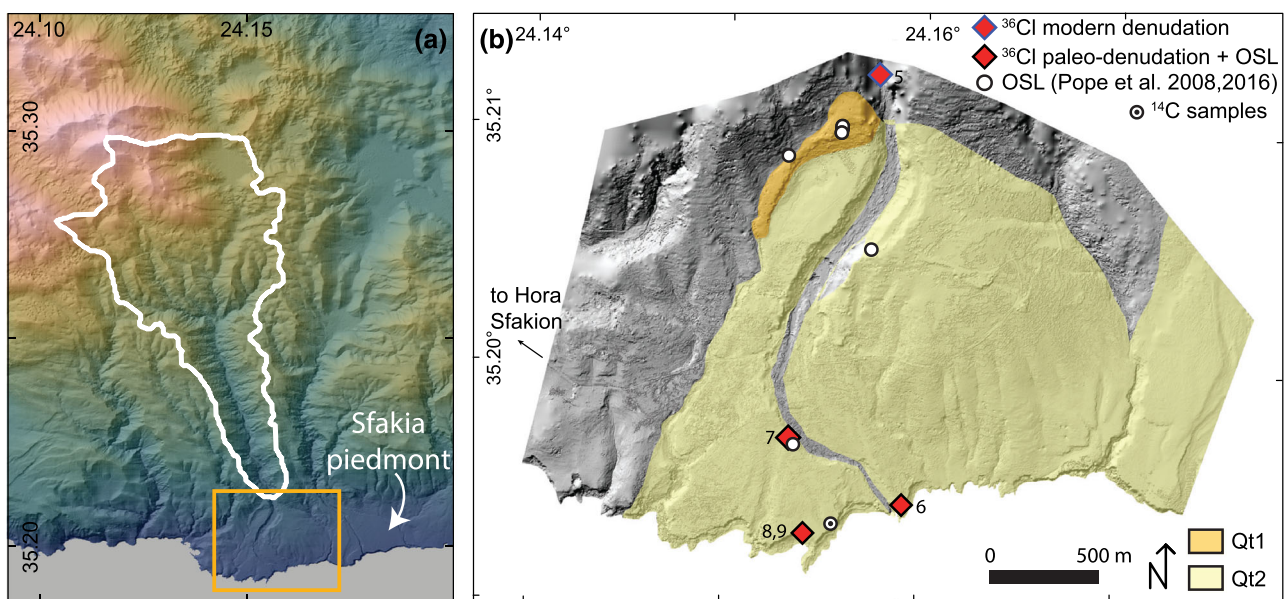


FIGURE 6 (a) Topography of Sfakia catchment with the box outlining the extent of (b). (b) Overview of Sfakia fan and sampling locations. The numbers of denudation rate samples correspond to Table 4. [Color figure can be viewed at wileyonlinelibrary.com]

term uplift. Platforms with elevations ranging from 46 to 56 m likely correlate with our paleoshorelines mapped at 53 m, platforms with elevations of 13–23 m probably correspond to the paleoshoreline mapped at 23 m elevation, and platforms between 0 and 9 m are linked to the historic uplift in the first centuries AD.

4.2 | Sfakia fan depositional chronology

As mentioned in Section 2, published geochronologic ages from the Sfakia fan show Qt1 deposition during MIS 5 and, after a short period of incision, Qt2 deposition from MIS 4 to 2 (Pope et al., 2008, 2016)

(Figure 6). Currently, both units are being incised by the active channel, with up to 45 m of incision into Qt2 (Figures 7a and c). Incision commenced between 5.5 and 11.2 ka (Pope et al., 2008), and we dated nine carbonate cement rinds from the uppermost distal section of the fan (Figures 6 and 7d) to improve these estimates. The calibrated age ranges show a large spread from 3.7 to 11.1 ka (Table 2). The age spread is likely related to multiple periods of cement formation (Geyh & Eitel, 1997). Moreover, the ‘hard-water effect’ that describes the incorporation of ‘dead’ carbon from local bedrock could bias the ages by up to one half-life (Shotton, 1972). Therefore, we use the oldest cement ages to estimate fan surface abandonment in our alternative burial scenario (supplement) but apply



FIGURE 7 Sfakia fan images and sampling locations. (a) Overview of fan head with Qt1 unit outlined by the dashed line and inset Qt2 fan deposits. (b) Sea cliffs eroded into the distal Qt2 fan deposits. (c) 45 m-thick section of Qt2 stratigraphy exposed in deeply incised feeder channel. (d) Carbonate clasts in the fan deposit are cemented by brown calcite cement, which we use for radiocarbon dating. (e) Section dated by Pope et al. (2008). Note hammer for scale. (f) Sea cliff in the Qt2 fan. The base of this section is shown in (e). [Color figure can be viewed at wileyonlinelibrary.com]

the conservative 5.5–11.2 ka Qtz abandonment time range for the post-burial correction of Sfakia paleo-denudation samples.

4.3 | Paleo-denudation rates

We estimate post-burial production for all cosmogenic nuclide samples (Figure 8, Table 3, Figures S2 and S3) to calculate paleo-denudation rates. For most samples, our estimated post-burial production is <30% of the total concentration; only for sample Sf-919-12, we estimate that 44% of the measured ^{10}Be and nearly half of the measured ^{36}Cl concentration can be explained by production after deposition (Figure 8, Table 4). For samples EI-919-3 and EI-919-4 from the Chrissoskalitissa fan, the post-burial ^{36}Cl production is probably high. However, the uncertainties are large due to the high concentration (~300 ppm) of natural Cl. The calculation of post-burial production with our alternative burial scenarios shows that the difference in the final concentrations is <10% (Table S3).

We calculated (paleo-)denudation rates from our post-burial-corrected concentrations (Table 4, Figure 9). Denudation rates range from 108 to 1421 mm/ka, excluding the Chrissoskalitissa sample that yielded a concentration too low for a denudation rate calculation. At the Stomio River in the Elafonisi fan system, the modern denudation rate is 108 ± 10 mm/ka. Paleo-denudation rates are higher (136 ± 27 and 159 ± 44 mm/ka) but overlap at one-sigma uncertainty. The paleo-denudation rate from MIS 4 at the Livadia fan system is higher (343 ± 116 mm/ka), but from a significantly smaller catchment (Figure 2). At the Chrissoskalitissa fan, high concentrations of natural Cl cause large uncertainties in the post-burial production. The post-burial-corrected concentration of sample EI-919-5 was too low for a denudation rate calculation. ^{36}Cl -derived paleo-denudation rates appear to be higher during MIS 2 compared to modern rates, yet due to the larger uncertainty in production rates, the modern and 23 ka paleo-denudation rates overlap within uncertainty.

At the Sfakia fan, most paleo-denudation rates are similar to modern rates, with some notable exceptions. The denudation rates from ^{10}Be and ^{36}Cl measurements agree for the modern stream sediment (264 ± 24 and 236 ± 20 mm/ka, respectively). However, three out of four ^{10}Be paleo-denudation rates are offset to lower values than the respective ^{36}Cl rates (Figure 9). ^{10}Be -derived denudation rates are similar to or slower than modern rates during MIS 2 and were faster at the MIS 3/4 boundary. ^{36}Cl -derived denudation rates show the same pattern but are offset to larger values.

Nuclide accumulation during denudation predicts a $^{36}\text{Cl}/^{10}\text{Be}$ ratio that is dependent on the denudation rate and the sample-specific chemistry. We calculated the predicted ratios for a range of plausible denudation rates (50–500 mm/ka) and production parameter uncertainties (Figure 10). Apart from the modern sample, all samples exhibit $^{36}\text{Cl}/^{10}\text{Be}$ ratios below the expected values. A prolonged deep sample burial can explain ratios larger than expected due to the greater percentage of muon production for ^{36}Cl . Alternatively, long and shallow (20–200 cm) sample material burial can reduce the ratio (~3.5 to 6 depending on sample composition). However, our independent constraints on aggradation and incision do not allow for significant burial at depths shallow enough to significantly reduce the $^{36}\text{Cl}/^{10}\text{Be}$ ratios. Another explanation for a low $^{36}\text{Cl}/^{10}\text{Be}$ ratio is the incomplete removal of meteoric ^{10}Be from our chert samples. It has previously been shown that adsorbed ^{10}Be can be challenging to remove from chert and lead to an excess of ^{10}Be (Zerathe et al., 2013). Without any other reasonable explanation, we assume that the incomplete removal of adsorbed ^{10}Be from the amorphous silicates led to the low $^{36}\text{Cl}/^{10}\text{Be}$ ratios. Therefore, we focus on the ^{36}Cl -derived denudation rates in our interpretation of the Sfakia fan evolution.

5 | DISCUSSION

We investigated the aggradation and incision timing and past variations in denudation rates of two Mediterranean fan systems during

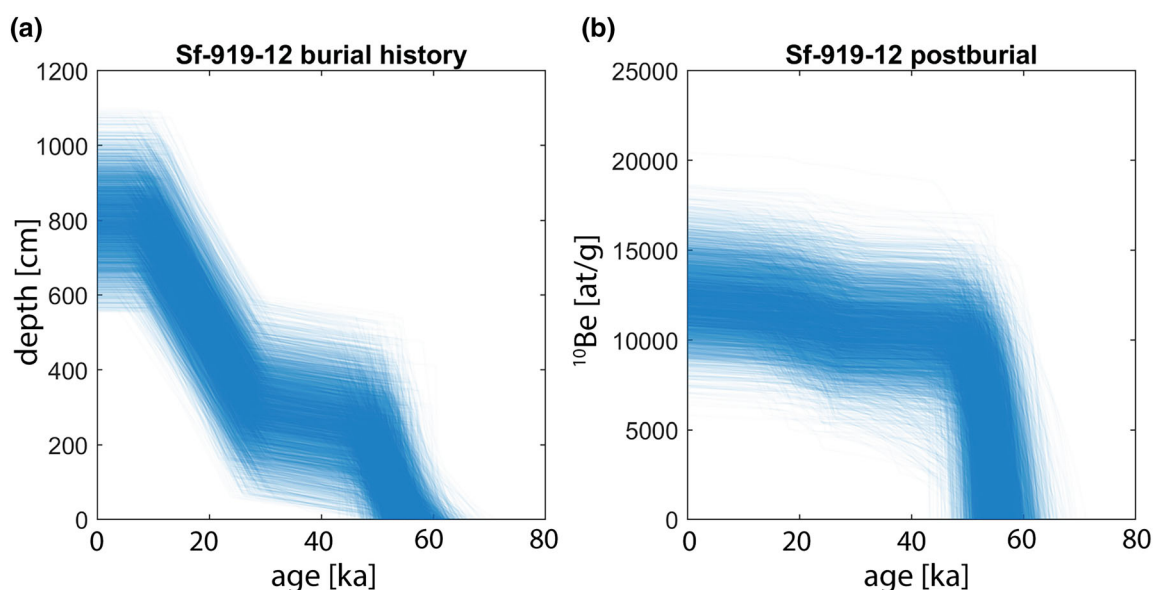


FIGURE 8 Calculation of post-burial nuclide accumulation for sample Sf-919-12. (a) Five thousand randomly sampled time–depth histories based on geochronologic ages and depth of overlying fan layers. (b) Forward models of nuclide accumulation due to post-burial production and radioactive decay were calculated with PostPro and based on the time–depth paths in (a). Concentrations start at zero because only the nuclide accumulation after burial is shown. [Color figure can be viewed at wileyonlinelibrary.com]

TABLE 4 Post-burial production estimates and paleo-denudation rates. The numbers in the first column correspond to the location numbers in Figures 2 and 5

| No. | Sample | Model surface age (ka) | Post-burial estimate (at/g) | Corrected ^{10}Be (at/g) | Erosion rate (mm/ka) |
|------------------|-----------------------|------------------------|-----------------------------|-----------------------------------|----------------------|
| ^{10}Be | | | | | |
| 1 | WC-616-7 [†] | 0 ± 0 | 0 ± 0 | 37 800 ± 2400 | 108 ± 10 |
| 2 | EL-919-1 | 68.5 ± 12.6 | 4406 ± 2493 | 29 794 ± 5587 | 136 ± 27 |
| 3 | EL-919-2 | 53.8 ± 11.1 | 9702 ± 5676 | 25 798 ± 6944 | 159 ± 44 |
| 4 | EI-617-PE-4 | 56.3 ± 10.2 | 4914 ± 2722 | 10 686 ± 3629 | 343 ± 116 |
| 5 | Sf-919-1 | 0 ± 0 | 0 ± 0 | 24 353 ± 1441 | 264 ± 24 |
| 6 | Sf-919-11 | 8.6 ± 2 | 3972 ± 1745 | 31 815 ± 2633 | 200 ± 22 |
| 7 | Sf-919-12 | 8.6 ± 2 | 12 408 ± 1902 | 15 259 ± 2388 | 414 ± 68 |
| 8 | Sf-919-14 | 8.6 ± 2 | 2578 ± 990 | 57 968 ± 2633 | 110 ± 9 |
| 9 | Sf-919-15 | 8.6 ± 2 | 2584 ± 1047 | 24 574 ± 1860 | 259 ± 26 |
| ^{36}Cl | | | | | |
| 10 | EI-919-3 | 0 ± 0 | 0 ± 0 | 76 000 ± 12 317 | 866 ± 193 |
| 11 | EI-919-4 | 13 ± 1.7 | 72 801 ± 36 741 | 58 199 ± 39 638 | 1421 ± 807 |
| 12 | EI-919-5 | 13 ± 1.7 | 92 157 ± 38 625 | 843 ± 40 932 | |
| 5 | SF-919-1 | 0 ± 0 | 0 ± 0 | 195 000 ± 12 030 | 236 ± 20 |
| 6 | SF-919-11 | 8.6 ± 2 | 31 099 ± 11 439 | 173 901 ± 16 005 | 266 ± 28 |
| 7 | SF-919-12 | 8.6 ± 2 | 95 997 ± 13 720 | 106 003 ± 17 900 | 422 ± 74 |
| 8 | SF-919-14 | 8.6 ± 2 | 23 408 ± 7715 | 274 592 ± 19 899 | 182 ± 17 |
| 9 | SF-919-15 | 8.6 ± 2 | 20 337 ± 6894 | 166 663 ± 12 226 | 263 ± 24 |

[†]Sample measured by Ott et al. (2019a).

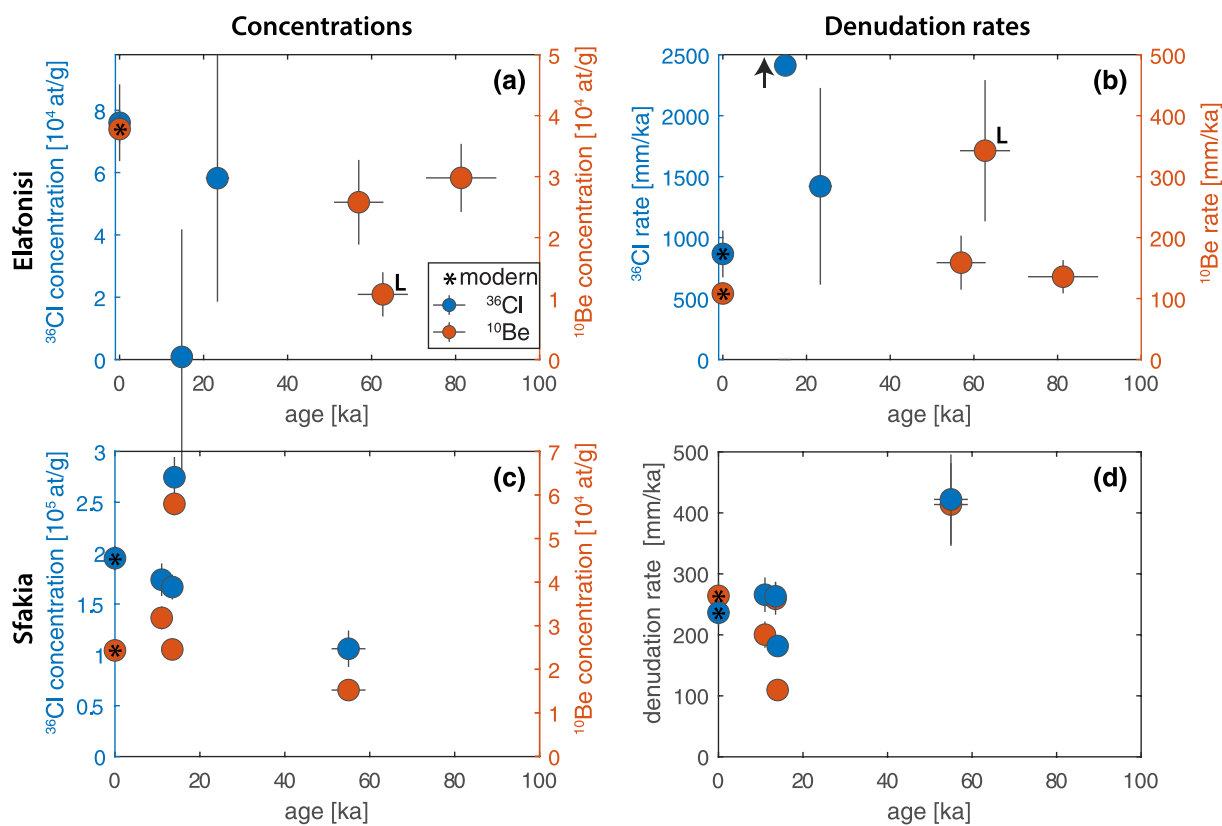


FIGURE 9 Post-burial corrected concentrations and (paleo-)denudation rates from Elafonisi and Sfakia fans. L = Livadia fan. One of the denudation rates in panel (b) from the Chrissisoskalitissa fan could not be calculated because the concentration was too low. Therefore, the denudation rate is assumed to be high, as indicated by the arrow. Samples from modern stream sediment are indicated with an asterisk (*). [Color figure can be viewed at wileyonlinelibrary.com]

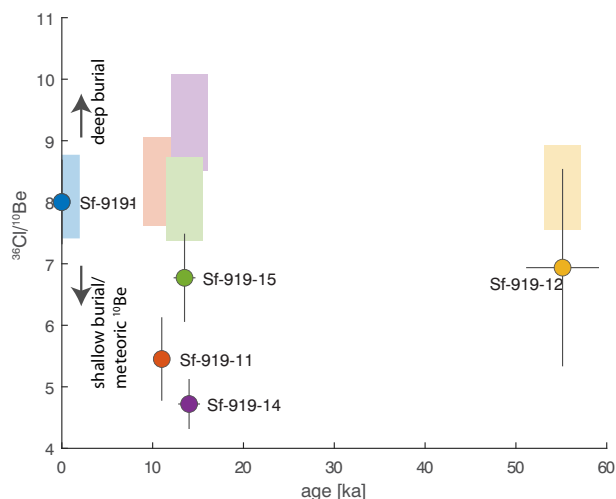


FIGURE 10 ^{36}Cl – ^{10}Be nuclide ratios of Sfakia fan samples. The shaded boxes indicate the theoretical range of nuclide ratios for erosion rates between 50 and 500 mm/ka. Deep (>3 m) burial within an alluvial fan would shift the ratios to greater values. The expected nuclide ratios vary between samples because the ^{36}Cl production depends on the sample chemistry. [Color figure can be viewed at wileyonlinelibrary.com]

the last glacial–interglacial climate cycle. Below, we first discuss the controls on aggradation and incision in our alluvial systems before discussing our paleo-denudation rates. Subsequently, we examine regional changes in climate, sea level, and vegetation throughout the same period and discuss the dominant factors driving changes within these alluvial systems.

5.1 | Timing of aggradation and incision

Our geochronologic data show that aggradation at the Elafonisi fan sequence occurred during MIS 5b/a (Qt2), MIS 4 to early MIS 3 (Qt3), and MIS 2 (Qt4) (Figure 4). At the Stomio River mouth, no Qt4 deposit is preserved. Due to its large catchment area, we assume that the Stomio River was able to incise substantially during the low sea level of MIS 2 and likely deposited an MIS 2 fan that now lies offshore. This scenario is supported by the embayment of the coastline directly at the Stomio River mouth (Figure 2), which suggests river incision during eustatic regression. We did not date Qt1; however, the steep fan-surface gradient suggests deposition during low sea levels. Based on its gradient and the other aggradation events broadly coinciding with the end of stadials, we assume the deposition of Qt1 during MIS 6. Incision events at the Elafonisi fan broadly coincide with interstadials and interglacial of MIS 1, 3, and 5a.

In contrast to the Elafonisi fan sequence, the Sfakia fan aggraded during most of the past glacial cycle (Pope et al., 2016). However, changes in the aggradation rate may still exist that we can derive from the dated sedimentary cross-sections published by Pope et al. (2008, 2016) (Figure 11). Combined with accumulation rates from the Chrissoskalitissa fan, dated in this study, aggradation was faster during late MIS 5 and 4 (90–60 ka), and especially during MIS 2 (29–14 ka) (Figure 11a). During MIS 1, all fan sections are being incised. However, we note that apparent aggradation rates are typically affected

by the timespan of measurement (Sadler, 1981). The timespans represented by our aggradation rates span one order of magnitude and show a moderate decrease with increasing timescale. We thus corrected the aggradation rates for a potential ‘Sadler effect’ by fitting a power law through the time scale–aggradation rate data (e.g. Gallen et al., 2015) (Figure 11b). Subsequently, we used this power-law fit to correct the aggradation rates in Figure 11a. For every aggradation measurement, we calculated an expected aggradation rate based on the power-law fit and subtracted the expected aggradation rate from the measured one (Figure 11c), similar to the approach of Kemp et al. (2020). These timescale-corrected relative aggradation rates show fast aggradation during MIS 4 and 2 and low rates during early MIS 5 and 3.

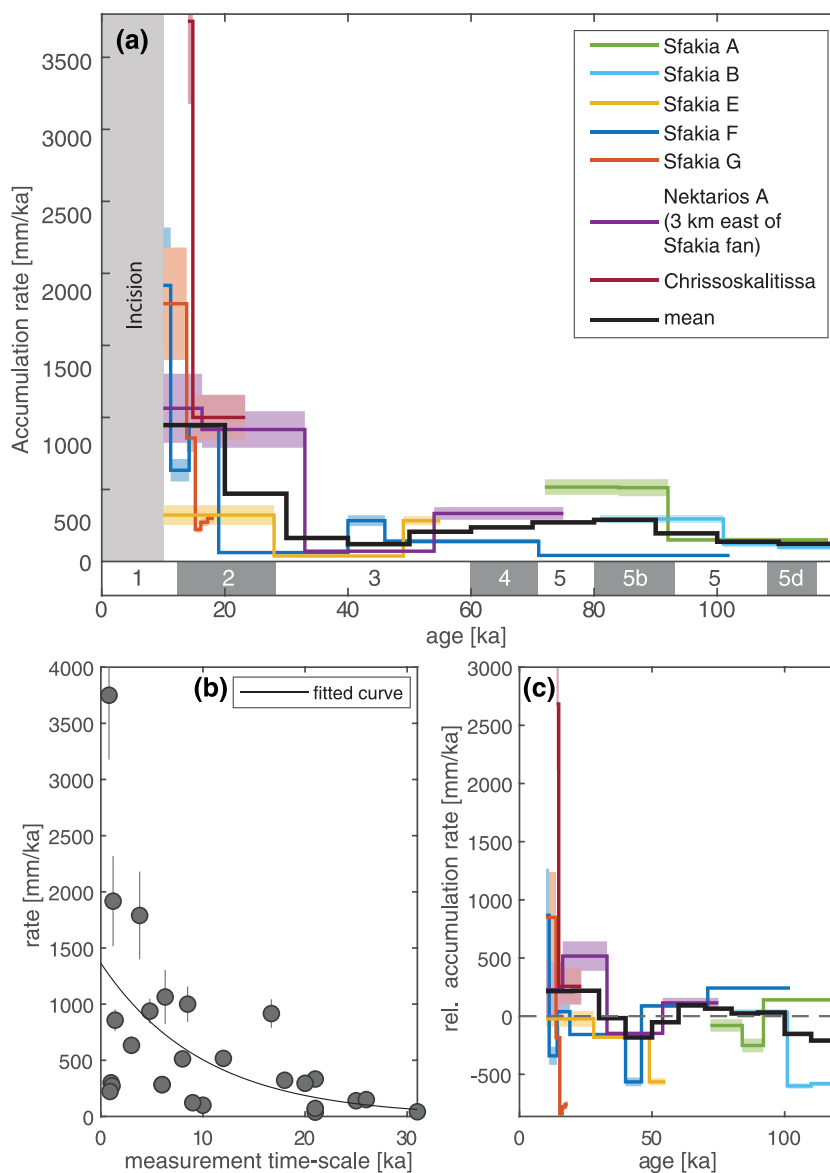
We thus conclude that at both study sites, aggradation increased during or towards the end of stadials (MIS 2, 4, 6), and incision or a reduction in aggradation rate occurred during interstadials and interglacials (MIS 1, 3, 5). Additionally, we compiled all geochronologic ages from Pleistocene alluvial fans and river terraces on Crete ($n = 49$, Figure 12a). The summed probability density distribution indicates two distinct peaks of aggradation ages, which correspond to MIS 2 and 4 (Figure 12a) and align well with the timing of increased aggradation at the study sites.

5.2 | Paleo-denudation rates

Our paleo-denudation rates are slightly elevated compared to modern denudation rates, although most differences are within the margin of error (Figure 9). The elevated uncertainty of the reported paleo-denudation rates is partly due to the uncertainty in post-burial nuclide accumulation. However, the largest uncertainties arise from the high [Cl] content of the three samples at Chrissoskalitissa, where large uncertainty on thermal and epithermal neutron production rates complicates the interpretation of changes in denudation rate. In most other samples, the post-burial production component is minor, and even the two depositional scenarios we examined for several samples show a <10% difference in paleo-denudation rates. Therefore, we assume our paleo-denudation rate estimates to be robust.

At the Elafonisi fan system, paleo-denudation rates along the Stomio River are within the error of the modern rates measured. The denudation rates in the small Livadia and Chrissoskalitissa fan catchments ($\sim 1.5 \text{ km}^2$ drainage area each) are greater by a factor of 3–9 compared to the Stomio River (35 km^2). The Chrissoskalitissa catchment is steeper (32°) than the Livadia (25°) and Stomio (26°) catchments and could explain why this location yields the fastest reported denudation rate so far for Crete (Ott et al., 2019a). However, both small catchments yield fast denudation rates, suggesting that the catchment area plays a role in the measured concentrations. In particular, the low paleo-denudation rates at Chrissoskalitissa could be explained by stochastic, low-concentration sediment input from mass wasting (Niemi et al., 2005). The Chrissoskalitissa catchment contains significant gypsum bedrock, which could promote slope failures. Aggradation due to landsliding has been shown to occur in a similar carbonate catchment on Crete (Bruni et al., 2021). However, CRN denudation rates measured elsewhere have been demonstrated to be accurate and consistent, despite significant landsliding within

FIGURE 11 Accumulation rates of stratigraphic sections published in Pope et al. (2008, 2016) from the Sfakia fans combined with accumulation rates from the Chrissoskalitissa fan. (a) Accumulation rates through time for the different sections. The black line represents the mean of 10 ka bins. (b) Relationship between measurement interval and accumulation rate with a power-law fit. (c) Relative accumulation rates were corrected for timescale bias with the power-law fit from (b). [Color figure can be viewed at [wileyonlinelibrary.com](https://onlinelibrary.wiley.com)]



catchments (Roda-Boluda et al., 2019), suggesting that mass wasting may not necessarily bias denudation-rate measurements. Alternatively, the shorter catchment length scale combined with fast denudation rates at Chrissoskalitissa could promote a more rapid response of this catchment to changes in climate compared to larger catchments (Castellort & Van Den Driessche, 2003; Tofelde et al., 2017; Wickert & Schildgen, 2019). If correct, prolonged sediment mixing and longer sediment transport times in the Stomio River and Sfakia catchment might have damped any climate-driven changes in denudation rate during sediment transport from source to sink. However, the integration times of our paleo-denudation rates are short (<5 ka, Figure 12c) and sediment storage within the catchments is minor; therefore, it remains unclear whether sediment mixing and storage might have obscured a climate signal.

Our (paleo-)denudation rates are lower than Late Pleistocene coastal uplift rates along Crete's south and west coast (Figure 5; Ott et al., 2019b). This discrepancy suggests that western Crete experienced net surface uplift during the Late Pleistocene, the rate of which we can crudely estimate by subtracting average denudation from coastal uplift rates. At the Sfakia fan, an average denudation rate of ~ 0.3 mm/a and the average coastal uplift rate at the Levka Ori of

0.8 mm/a (Ott et al., 2019b) suggest 0.5 mm/ka of Levka Ori surface uplift. At Elafonisi, an average denudation rate of ~ 0.5 mm/a, and an ~ 1.3 mm/a coastal uplift rate (Figure 5), result in a surface uplift rate of ~ 0.8 mm/a. Higher surface uplift rates in western Crete are consistent with a proposed Late Pleistocene acceleration in uplift inferred along the west coast (Ott et al., 2019b). If these surface uplift rates were constant through time, the 2.5 km elevation of the Levka Ori could have been built within the past 5 Ma, consistent with the island-wide uplift and emergence recorded at the Miocene–Pliocene boundary (van Hinsbergen & Meulenkaamp, 2006).

5.3 | Linking aggradation, incision, and denudation to base level, climate, and vegetation

Periods of pronounced aggradation align with stadials—sea-level lowstands—during the last glacial cycle (MIS 2, 4, 5b). Low sea level during these periods should favour incision in response to a base-level fall and seaward shift of alluvial depocentres. The brief period of incision observed at both study sites at the MIS 5a/4 transition might be an example of such base-level controlled entrenchment. However,

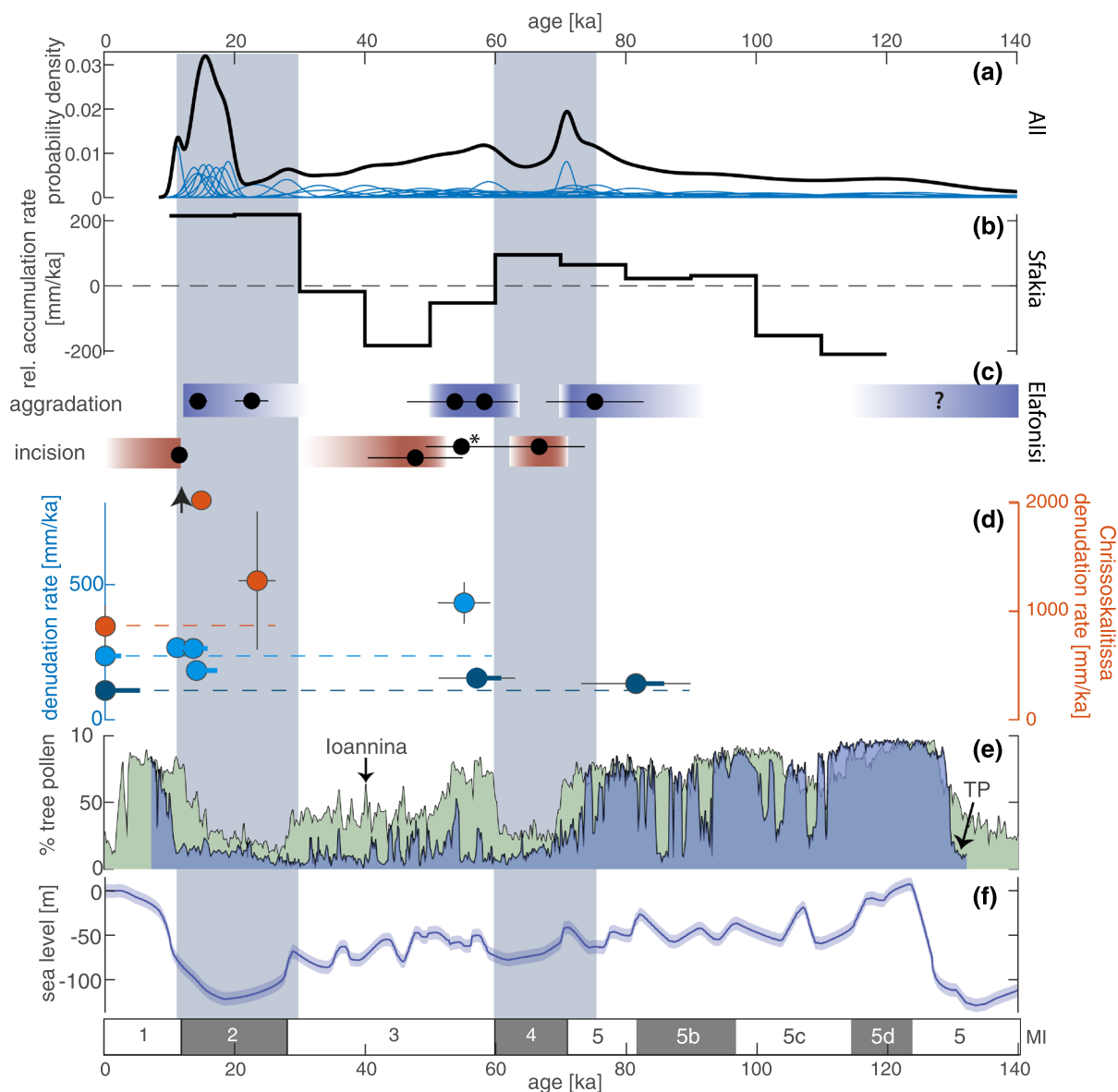


FIGURE 12 Summary of aggradation and paleo-denudation data. (a) Individual (blue) and summed probability density functions of compiled geochronologic ages from alluvial fans on Crete (this study; Gallen et al., 2014; Holcomb et al., 2021; Pope et al., 2008, 2016). (b) Mean relative sediment accumulation rate from Figure 11C. (c) Aggradation and incision constraints from Elafonisi. (d) Paleo-denudation rates from this study. The Chrisoskaliitissa (orange) denudation rates are scaled to the right y-axis for visibility. Rates from the Sfakia fan (light blue) and Stomio River (dark blue) are scaled to the left axis. Thick lines behind the dots indicate the approximate integration time of the cosmogenic nuclide sample. Dashed lines correspond to modern reference values. (e) Percentage of total tree pollen from Tenaghi-Philippon (TP, blue) in the northern Aegean (Wulf et al., 2018) and Ioannina (green) in northwest Greece (Roucoux et al., 2011). We calculated our age model for the Ioannina data based on linear interpolation between dated layers. Hence, the Ioannina pollen record's age uncertainty is greater than Tenaghi-Philippon. (f) Sea-level curve by Lambeck and Chappell (2001). [Color figure can be viewed at wileyonlinelibrary.com]

incision occurring during sea-level highstands (MIS 1 and 3) suggests that eustasy is only a second-order control on the alluviation dynamics in coastal Crete.

Changes in tectonically induced base-level falls could also trigger incision. However, the uplift rates derived from paleoshorelines suggest rather constant uplift rates during the Late Pleistocene (Figure 5), which agrees with the findings of Ott et al. (2019b). Moreover, given that high-amplitude eustatic sea-level variations only had a limited influence on aggradation, it is unlikely that variations in tectonic rates controlled the aggradation behaviour during the Late Pleistocene.

Climate archives from the Eastern Mediterranean show substantial changes in temperature, precipitation, and vegetation throughout

the Late Pleistocene: dry and cold conditions during stadials contrast with warm and wet conditions during interstadials and interglacials (Langgut et al., 2011; Wulf et al., 2018). We hypothesize that such variations in climate are the main control on the aggradation and incision behaviour of the studied fans and dominate the influence of base-level variations.

Aggradation during stadials and incision during interstadials has been observed in other Mediterranean regions (Macklin et al., 2002; Pope & Wilkinson, 2005; Wegmann & Pazzaglia, 2009; Zembo et al., 2009). For instance, Wegmann and Pazzaglia (2009) found that depending on the hillslope-derived sediment supply in the Northern Apennines, river aggradation or strath terrace formation occurred

during stadials with subsequent incision during the transition to interstadials. A compilation of aggradation periods in the Mediterranean by Macklin et al. (2002) documents major aggradation during MIS 6, the MIS 5b/a transition, MIS 4, MIS 2, and universal incision during MIS 1 at all studied sites. These aggradation periods align with the aggradation at the Elafonsi fan system and periods of increased aggradation at the Sfakia fan. About half of the sites in the Macklin et al. (2002) compilation lie inland. Therefore, the temporal correlation of aggradation and incision in the Eastern Mediterranean is additional evidence that both are mostly governed by climate-related changes in sediment transport, with only second-order controls by tectonics and sea level.

The aggradation behaviour of rivers on orbital time scales is a function of sediment supply and runoff-controlled transport capacity. Our paleo-denudation rates show that hillslope denudation remained fairly constant throughout the glacial cycle, suggesting no major changes in hillslope denudation during the variations in aggradation and incision. This observation is in agreement with findings from the Northern Apennines, Central Europe, and the Himalayas, where Pleistocene denudation rates remain relatively stable (Cyr & Granger, 2008; Kapannusch et al., 2020; Schaller et al., 2002), despite shifts in river aggradation and incision (Wegmann & Pazzaglia, 2009). However, the fluctuations in precipitation observed by paleoclimate studies in Greece suggest major variations in runoff-controlled stream transport capacity during the same time. We thus hypothesize that increased transport capacity due to wet conditions during interstadials and interglacials is probably the main driver of stream incision, whereas reduced transport capacity during stadials led to aggradation. This interpretation suggests that streams in western Crete are transport-limited and sensitive to hydroclimate fluctuations.

Climate changes also led to large fluctuations in vegetation, which may impact sediment supply. Pollen records from northern Greece (Figure 12e) and Israel show forest dominance during interstadials and interglacials and a switch to steppe conditions during stadials (Langgut et al., 2011; Margari et al., 2009; Roucoux et al., 2011; Wulf et al., 2018). Vegetation changes could have modulated the sediment supply to the channel by stabilizing hillslope material (Amundson et al., 2015; Torres Acosta et al., 2015). Therefore, shifts from forest to steppe conditions during stadials may have released pulses of hillslope sediment, leading to aggradation, similar to what can be observed in numerical simulations by Tucker and Slingerland (1997). Faster hillslope transport due to less vegetation would decrease the measured cosmogenic nuclide concentrations (Anderson, 2015). However, this effect may be buffered by (1) the initial release of higher-concentration material that was stabilized, (2) sediment mixing within the catchment, which may dilute the input of low-concentration material from the hillslopes, and (3) the sluggish decrease in CRN concentration due to the integration time of CRNs. Our more variable paleo-denudation rates from the small Chrissoskalitissa fan could indicate that small catchments with high denudation rates may be capable of registering a short-lived increase in denudation. In the larger Stomio River and Sfakia catchments, sediment storage is limited and integration times of cosmogenic nuclides are short (Figure 12d). Yet, the addition of various buffering effects may be sufficient to damp a signal in cosmogenic nuclide-derived denudation rates to within uncertainty of modern rates, as observed in this study. Hence, it is likely that the large shifts in vegetation contributed to aggradation and incision by releasing and withholding hillslope sediment, respectively; however, the uncertainties and limited number of our paleo-

denudation rates do not allow us to infer if changes in hillslope denudation played a secondary role in the aggradation behaviour of streams and alluvial fans.

Relatively steady hillslope denudation during aggradation–incision events has also been observed in the Himalayas (Kapannusch et al., 2020). A numerical model of 1-D alluvial river evolution by Simpson and Castellort (2012) showed that variations in water discharge get amplified and transmitted downstream, leading to periods of pronounced aggradation and incision. In contrast, fluctuations in sediment discharge get damped on their way from source to sink. Our observations agree well with these findings. Observed variations in sediment input on Crete were minor and, if present, appear to have been damped over a length scale of a few kilometres. However, variations in hydroclimate left a strong imprint on the studied coastal alluvial systems, even outcompeting high-amplitude variations in sea level. The consistency between our data, theoretical expectations, and a few other studies suggests that alluvial sequences may rather record variations in hydroclimate than sediment input in many environments.

6 | SUMMARY AND CONCLUSIONS

Quaternary alluvial deposits at the Elafonsi fan complex, Crete, Greece, were deposited during MIS 2, 4, 5a/b, and likely also MIS 6. Similarly, aggradation rates at the Sfakia fan suggest the fastest deposition during MIS 2 and 4, with a brief period of minor incision at the MIS 5a/4 boundary and major incision during MIS 1. Despite large variations in aggradation and incision, millennial-scale denudation rates remained relatively constant in western Crete during the Late Pleistocene, except for one small catchment with elevated rates during MIS 2.

Periods of aggradation coincide with dry climate and steppe vegetation. We therefore attribute temporal changes in aggradation primarily to decreased runoff, potentially supported by a transient increase in hillslope sediment release due to a decline in vegetation cover. Major incision during MIS 1 is likely a response to increased rainfall and stream-transport capacity alongside denser vegetation stabilizing hillslope material. An early period of incision at the MIS 5a/4 transition likely occurred in response to rapid sea-level fall, suggesting that base level-driven incision events are superposed onto the climatically driven sequence of aggradation and incision.

Hence, we find that streams in western Crete show transport-limited behaviour, where variations in hydroclimate primarily modulate aggradation and incision while millennial-scale denudation rates remain relatively constant. In accordance with numerical models, we speculate that sediment-supply variations are only recorded in small and rapidly eroding basins, while changes in runoff dominate the alluvial record.

ACKNOWLEDGEMENTS

We thank Negar Haghypour, ETH Zürich for assistance during ^{10}Be sample preparation and ^{14}C measurements. Richard F. Ott is funded by the Swiss National Science Foundation, grant number P2EZP2_191866. We thank Hellenic Cadastre SA for DEM data. Sincere thanks to Christina Tsimi (NOA) for customizing the 5 m digital elevation models for the research area. We thank Emma Lodes for designing the graphical abstract. Open Access funding enabled and organized by Projekt DEAL.

CONFLICT OF INTEREST

The authors declare no conflict of interest.

AUTHOR CONTRIBUTIONS

RFO conceptualized the study, the methodology, and developed the software.

RFO, DS, KWW, MKD, SIO, RJP, CV, TMM, and MC conducted the investigation.

RFO wrote the manuscript with input from all co-authors.

DATA AVAILABILITY STATEMENT

The PostPro software package is available at <https://doi.org/10.5880/GFZ.3.3.2022.002> together with a user guide and the data presented in this publication as input for the code. All other data are available within this manuscript and the online supplement.

ORCID

Richard F. Ott  <https://orcid.org/0000-0002-8257-0079>

Marcus Christl  <https://orcid.org/0000-0002-3131-6652>

REFERENCES

- Adamic, G. & Aitken, M.J. (1998) Dose-rate conversion factors: Update. *Ancient TL*, 16, 37–50.
- Aitken, M.J. (1998) *An Introduction to Optical Dating: The Dating of Quaternary Sediments by the Use of Photon-Stimulated Luminescence*. Oxford: Oxford University Press.
- Amundson, R., Heimsath, A., Owen, J., Yoo, K. & Dietrich, W.E. (2015) Hillslope soils and vegetation. *Geomorphology*, 234, 122–132. Available from: <https://doi.org/10.1016/J.GEOMORPH.2014.12.031>
- Anderson, R.S. (2015) Particle trajectories on hillslopes: Implications for particle age and ¹⁰Be structure. *Journal of Geophysical Research – Earth Surface*, 119, 1–20. Available from: <https://doi.org/10.1002/2013JF002950>
- Angelier, J. (1979) Recent Quaternary tectonics in the Hellenic Arc: Examples of geological observations on land. *Tectonophysics*, 52(1–4), 267–275. Available from: [https://doi.org/10.1016/0040-1951\(79\)90231-2](https://doi.org/10.1016/0040-1951(79)90231-2)
- Beck, H.E., Zimmermann, N.E., McVicar, T.R., Vergopolan, N., Berg, A. & Wood, E.F. (2018) Present and future Köppen–Geiger climate classification maps at 1-km resolution. *Scientific Data*, 5, 1–12. Available from: <https://doi.org/10.1038/sdata.2018.214>
- Berger, A.L., Gulick, S.P.S., Spotila, J.A., Upton, P., Jaeger, J.M., Chapman, J.B., Worthington, L.A., Pavlis, T.L., Ridgway, K.D., Willems, B.A. & McAleer, R.J. (2008) Quaternary tectonic response to intensified glacial erosion in an orogenic wedge. *Nature Geoscience*, 1(11), 793–799. Available from: <https://doi.org/10.1038/ngeo334>
- Bierman, P.R., Caffee, M.W., Davis, P.T., Marsella, K., Pavich, M., Colgan, P., Mickelson, D. & Larsen, J. (2002) Rates and timing of earth surface processes from in situ-produced cosmogenic Be-10. *Reviews in Mineralogy and Geochemistry*, 50(1), 147–205. Available from: <https://doi.org/10.2138/rmg.2002.50.4>
- Bruni, E.T., Ott, R.F., Picotti, V., Haghpor, N., Wegmann, K.W. & Gallen, S.F. (2021) Stochastic alluvial fan and terrace formation triggered by a high-magnitude Holocene landslide in the Klados Gorge, Crete. *Earth Surface Dynamics (Pembroke, Ont.)*, 9(4), 771–793. Available from: <https://doi.org/10.5194/esurf-9-771-2021>
- Bull, W.B. (1991) *Geomorphic Responses to Climatic Change*. New York: Oxford University Press.
- Castelltort, S. & Van Den Driessche, J. (2003) How plausible are high-frequency sediment supply-driven cycles in the stratigraphic record? *Sedimentary Geology*, 157(1–2), 3–13. Available from: [https://doi.org/10.1016/S0037-0738\(03\)00066-6](https://doi.org/10.1016/S0037-0738(03)00066-6)
- Cheddadi, R. & Rossignol-Strick, M. (1995) Eastern Mediterranean quaternary paleoclimates from pollen and isotope records of marine cores in the Nile cone area. *Paleoceanography*, 10(2), 291–300. Available from: <https://doi.org/10.1029/94PA02672>
- Christl, M., Vockenhuber, C., Kubik, P.W., Wacker, L., Lachner, J., Alfimov, V. & Synal, H.-A. (2013) The ETH Zurich AMS facilities: Performance parameters and reference materials. *Nuclear Instruments and Methods in Physics Research, Section B: Beam Interactions with Materials and Atoms*, 294, 29–38. Available from: <https://doi.org/10.1016/j.nimb.2012.03.004>
- Coltorti, M. & Dramis, F. (1995) The chronology of Upper Pleistocene stratified slope-waste deposits in Central Italy. *Permafrost and Periglacial Processes*, 6(3), 235–242. Available from: <https://doi.org/10.1002/PPP.3430060304>
- Creutzberg, N., Drooger, C.W., Meulenkamp, J.E., Papastamatiou, J., Sannemann, W., Seidel, E. & Tatares, A. (1977) *General Geological Map of the Island of Crete*, 1:200,000. Institute of Geology and Mineral Exploration, Athens.
- Cyr, A.J. & Granger, D.E. (2008) Dynamic equilibrium among erosion, river incision, and coastal uplift in the northern and central Apennines, Italy. *Geology*, 36(2), 103–106. Available from: <https://doi.org/10.1130/G24003A.1>
- D'Arcy, M., Roda-Boluda, D.C. & Whittaker, A.C. (2017) Glacial-interglacial climate changes recorded by debris flow fan deposits, Owens Valley, California. *Quaternary Science Reviews*, 169, 288–311. Available from: <https://doi.org/10.1016/J.QUASCIREV.2017.06.002>
- D'Arcy, M., Whittaker, A.C. & Roda-Boluda, D.C. (2017) Measuring alluvial fan sensitivity to past climate changes using a self-similarity approach to grain-size fining, Death Valley, California. *Sedimentology*, 64(2), 388–424. Available from: <https://doi.org/10.1111/SED.12308>
- Dewald, A., Heinze, S., Jolie, J., Zilges, A., Dunai, T., Rethemeyer, J., Melles, M., Staubwasser, M., Kuczewski, B., Richter, J., Radtke, U., von Blanckenburg, F. & Klein, M. (2013) CologneAMS, a dedicated center for accelerator mass spectrometry in Germany. *Nuclear Instruments and Methods in Physics Research, Section B: Beam Interactions with Materials and Atoms*, 294, 18–23. Available from: <https://doi.org/10.1016/j.nimb.2012.04.030>
- Fassoulas, C., Kiliadis, A. & Mountrakis, D. (1994) Postnappe stacking extension and exhumation of high-pressure/low-temperature rocks in the island of Crete, Greece. *Tectonics*, 13(1), 127–138. Available from: <https://doi.org/10.1029/93TC01955>
- Ferrier, G. & Pope, R.J.J. (2012) Quantitative mapping of alluvial fan evolution using ground-based reflectance spectroscopy. *Geomorphology*, 175–176, 14–24. Available from: <https://doi.org/10.1016/J.GEOMORPH.2012.06.013>
- Galbraith, R.F. & Roberts, R.G. (2012) Statistical aspects of equivalent dose and error calculation and display in OSL dating: An overview and some recommendations. *Quaternary Geochronology*, 11, 1–27. Available from: <https://doi.org/10.1016/J.QUAGEO.2012.04.020>
- Gallen, S.F., Pazzaglia, F.J., Wegmann, K.W., Pederson, J.L. & Gardner, T. W. (2015) The dynamic reference frame of rivers and apparent transience in incision rates. *Geology*, 43(7), 623–626. <https://doi.org/10.1130/G36692.1>
- Gallen, S.F., Wegmann, K.W., Bohnenstiehl, D.R., Pazzaglia, F.J., Brandon, M.T. & Fassoulas, C. (2014) Active simultaneous uplift and margin-normal extension in a forearc high, Crete, Greece. *Earth and Planetary Science Letters*, 398, 11–24. Available from: <https://doi.org/10.1016/j.epsl.2014.04.038>
- Geyh, M.A. & Eitel, B. (1997) Radiometric dating of young and old calcrete. *Radiocarbon*, 40(2), 795–802. Available from: <https://doi.org/10.1017/S0033822200018749>
- Giresse, P. & Martzluft, M. (2015) AMS radiocarbon dating of carbonate cements in Late Pleistocene alluvial conglomerates, Verdoube River: Palaeoenvironmental implications concerning the Palaeolithic site of Tautavel (Pyrénées-Orientales). *Geomorphologie*, 21(2), 115–130. Available from: <https://doi.org/10.4000/GEOMORPHOLOGIE.10956>
- Guérin, G., Mercier, N. & Adamic, G. (2011) Dose-rate conversion factors: Update. *Ancient TL*, 29, 5–8.
- Hales, T.C. & Roering, J.J. (2007) Climatic controls on frost cracking and implications for the evolution of bedrock landscapes. *Journal of*

- Geophysical Research – Earth Surface*, 112(F2), 2033. Available from: <https://doi.org/10.1029/2006JF000616>
- Harvey, A.M., Silva, P.G., Mather, A.E., Goy, J.L., Stokes, M. & Zazo, C. (1999) The impact of Quaternary sea-level and climatic change on coastal alluvial fans in the Cabo de Gata ranges, southeast Spain. *Geomorphology*, 28(1–2), 1–22. Available from: [https://doi.org/10.1016/S0169-555X\(98\)00100-7](https://doi.org/10.1016/S0169-555X(98)00100-7)
- Herman, F., Seward, D., Valla, P.G., Carter, A., Kohn, B., Willett, S.D. & Ehlers, T.A. (2013) Worldwide acceleration of mountain erosion under a cooling climate. *Nature*, 504(7480), 423–426. Available from: <https://doi.org/10.1038/nature12877>
- Holcomb, J.A., Wegmann, K.W. & Runnels, C.N. (2021) Late Quaternary coastal stratigraphy at Mochlos Bay, northeast Crete, Greece: Implications for palaeolithic archaeological site preservation and hominin dispersals. In *Geological Society of America Abstracts with Programs*, v. 53. <https://doi.org/10.1130/abs/2021AM-369290>
- Hughes, P.D. & Woodward, J.C. (2017) Quaternary glaciation in the Mediterranean mountains: A new synthesis. *Geological Society of London, Special Publications*, 433(1), 1–23. Available from: <https://doi.org/10.1144/SP433.14>
- Ivy-Ochs, S., Synal, H.-A., Roth, C. & Schaller, M. (2004) Initial results from isotope dilution for Cl and ³⁶Cl measurements at the PSI/ETH Zurich AMS facility. *Nuclear Instruments and Methods in Physics Research, Section B: Beam Interactions with Materials and Atoms*, 223–224, 623–627. Available from: <https://doi.org/10.1016/j.nimb.2004.04.115>
- Jolivet, L. & Brun, J.-P. (2010) Cenozoic geodynamic evolution of the Aegean. *International Journal of Earth Sciences*, 99(1), 109–138. Available from: <https://doi.org/10.1007/s00531-008-0366-4>
- Kapannusch, R., Scherler, D., King, G. & Wittmann, H. (2020) Glacial influence on Late Pleistocene ¹⁰Be-derived paleo-erosion rates in the north-western Himalaya, India. *Earth and Planetary Science Letters*, 547, 116441. Available from: <https://doi.org/10.1016/j.epsl.2020.116441>
- Kemp, D.B., Sadler, P.M. & Vanacker, V. (2020) The human impact on North American erosion, sediment transfer, and storage in a geologic context. *Nature Communications*, 11, 1–9. Available from: <https://doi.org/10.1038/s41467-020-19744-3>
- Lajoie, K.R. (1986) Coastal tectonics. In: Wallace, R. (Ed.) *Active Tectonics*. Washington, DC: National Academy Press, pp. 95–124.
- Lambeck, K. & Chappell, J. (2001) Sea level change through the last glacial cycle. *Science*, 292(5517), 679–686. Available from: <https://doi.org/10.1126/science.1059549>
- Langgut, D., Almogi-Labin, A., Bar-Matthews, M. & Weinstein-Evron, M. (2011) Vegetation and climate changes in the south eastern Mediterranean during the last glacial–interglacial cycle (86 ka): New marine pollen record. *Quaternary Science Reviews*, 30(27–28), 3960–3972. Available from: <https://doi.org/10.1016/J.QUASCREV.2011.10.016>
- Lenard, S.J.P., Lavé, J., France-Lanord, C., Aumaitre, G., Bourlès, D.L. & Keddadouche, K. (2020) Steady erosion rates in the Himalayas through late Cenozoic climatic changes. *Nature Geoscience*, 13(6), 448–452. Available from: <https://doi.org/10.1038/s41561-020-0585-2>
- Macklin, M.G., Fuller, I.C., Lewin, J., Maas, G.S., Passmore, D.G., Rose, J., Woodward, J.C., Black, S., Hamlin, R.H.B. & Rowan, J.S. (2002) Correlation of fluvial sequences in the Mediterranean basin over the last 200 ka and their relationship to climate change. *Quaternary Science Reviews*, 21(14–15), 1633–1641. Available from: [https://doi.org/10.1016/S0277-3791\(01\)00147-0](https://doi.org/10.1016/S0277-3791(01)00147-0)
- Margari, V., Gibbard, P.L., Bryant, C.L. & Tzedakis, P.C. (2009) Character of vegetational and environmental changes in southern Europe during the last glacial period; evidence from Lesvos Island, Greece. *Quaternary Science Reviews*, 28(13–14), 1317–1339. Available from: <https://doi.org/10.1016/J.QUASCREV.2009.01.008>
- Mariotti, A., Blard, P.H., Charreau, J., Toucanne, S., Jorry, S.J., Molliex, S., Bourlès, D.L., Aumaitre, G. & Keddadouche, K. (2021) Nonlinear forcing of climate on mountain denudation during glaciations. *Nature Geoscience*, 14(1), 16–22. Available from: <https://doi.org/10.1038/s41561-020-00672-2>
- Marrero, S.M., Phillips, F.M., Borchers, B., Lifton, N., Aumer, R. & Balco, G. (2016a) Cosmogenic nuclide systematics and the CRONUScal program. *Quaternary Geochronology*, 31, 160–187. Available from: <https://doi.org/10.1016/j.quageo.2015.09.005>
- Marrero, S.M., Phillips, F.M., Caffee, M.W. & Gosse, J.C. (2016b) CRONUS-Earth cosmogenic ³⁶Cl calibration. *Quaternary Geochronology*, 31, 199–219. Available from: <https://doi.org/10.1016/j.quageo.2015.10.002>
- Marshall, J.A., Roering, J.J., Bartlein, P.J., Gavin, D.G., Granger, D.E., Rempel, A.W., Praskievicz, S.J. & Hales, T.C. (2015) Frost for the trees: Did climate increase erosion in unglaciated landscapes during the Late Pleistocene? *Science Advances*, 1(10), e1500715. Available from: <https://doi.org/10.1126/sciadv.1500715>
- Marshall, J.A., Roering, J.J., Rempel, A.W., Shafer, S.L. & Bartlein, P.J. (2021) Extensive frost weathering across unglaciated North America during the last glacial maximum. *Geophysical Research Letters*, 48(5), e2020GL090305. Available from: <https://doi.org/10.1029/2020GL090305>
- Mason, C.C. & Romans, B.W. (2018) Climate-driven unsteady denudation and sediment flux in a high-relief unglaciated catchment-fan using ²⁶Al and ¹⁰Be: Panamint Valley, California. *Earth and Planetary Science Letters*, 492, 130–143. Available from: <https://doi.org/10.1016/j.epsl.2018.03.056>
- Mountrakis, D., Kilias, A., Pavlaki, A., Fassoulas, C., Thomaidou, E., Papazachos, C., Papaioannou, C., Roumelioti, Z., Benetatos, C. & Vamvakaris, D. (2013) Neotectonic analysis, active stress field and active faults seismic hazard assessment in Western Crete. *Bulletin of the Geological Society of Greece*, 47(2), 582–594. Available from: <https://doi.org/10.12681/bgsg.1108>
- Murray, A.S. & Wintle, A.G. (2000) Luminescence dating of quartz using an improved single-aliquot regenerative-dose protocol. *Radiation Measurements*, 32(1), 57–73. Available from: [https://doi.org/10.1016/S1350-4487\(99\)00253-X](https://doi.org/10.1016/S1350-4487(99)00253-X)
- Nemec, W. & Postma, G. (1993) Quaternary alluvial fans in southwestern Crete: Sedimentation processes and geomorphic evolution. In: Marzo, M. & Puigdefabregas, C. (Eds.) *Alluvial Sedimentation*. Oxford: Blackwell Scientific, pp. 235–276.
- Niemi, N.A., Oskin, M., Burbank, D.W., Heimsath, A.M. & Gabet, E.J. (2005) Effects of bedrock landslides on cosmogenically determined erosion rates. *Earth and Planetary Science Letters*, 237(3–4), 480–498. Available from: <https://doi.org/10.1016/j.epsl.2005.07.009>
- Nishiizumi, K., Winterer, E., Kohl, C., Klein, J., Middleton, R., Lal, D., Arnold, J.R. & Jolla, L. (1989) Cosmic ray production rates of ¹⁰Be and ²⁶Al in quartz from glacially polished rocks. *Journal of Geophysical Research – Solid Earth*, 94(B12), 17907–17915. Available from: <https://doi.org/10.1029/JB094B12P17907>
- Ott, R.F. (2020) How lithology impacts global topography, vegetation, and animal biodiversity: A global-scale analysis of mountainous regions. *Geophysical Research Letters*, 47(20), Available from: <https://doi.org/10.1029/2020GL088649>
- Ott, R.F. (2022) POST PRO – POSTburial PROduction for cosmogenic nuclide samples. GFZ Data Services. <https://doi.org/10.5880/GFZ.3.3.2022.002>
- Ott, R.F., Gallen, S.F., Caves Rügenstein, J.K., Ivy-Ochs, S., Helman, D., Fassoulas, C., Vockenhuber, C., Christl, M. & Willett, S.D. (2019a) Chemical versus mechanical denudation in meta-clastic and carbonate bedrock catchments on Crete, Greece, and mechanisms for steep and high carbonate topography. *Journal of Geophysical Research – Earth Surface*, 124(12), 2943–2961. Available from: <https://doi.org/10.1029/2019JF005142>
- Ott, R.F., Gallen, S.F., Wegmann, K.W., Biswas, R.H., Herman, F. & Willett, S.D. (2019b) Pleistocene terrace formation, quaternary rock uplift rates and geodynamics of the Hellenic subduction zone revealed from dating of paleoshorelines on Crete, Greece. *Earth and Planetary Science Letters*, 525, 115757. Available from: <https://doi.org/10.1016/j.epsl.2019.115757>
- Ott, R.F., Wegmann, K.W., Gallen, S.F., Pazzaglia, F.J., Brandon, M.T., Ueda, K. & Fassoulas, C. (2021) Reassessing eastern Mediterranean tectonics and earthquake hazard from the 365 CE earthquake. *AGU*

- Advances*, 2(2), e2020AV000315. Available from: <https://doi.org/10.1029/2020AV000315>
- Peizhen, Z., Molnar, P. & Downs, W.R. (2001) Increased sedimentation rates and grain sizes 2–4 Myr ago due to the influence of climate change on erosion rates. *Nature*, 410, 891–897. Available from: <https://doi.org/10.1038/35073504>
- Phillips, F.M., Argento, D.C., Balco, G., Caffee, M.W., Clem, J., Dunai, T.J., Finkel, R., Goehring, B., Gosse, J.C., Hudson, A.M., Jull, A.J.T., Kelly, M.A., Kurz, M., Lal, D., Lifton, N., Marrero, S.M., Nishiizumi, K., Reedy, R.C., Schaefer, J., Stone, J.O.H., Swanson, T. & Zreda, M.G. (2016) The CRONUS-Earth project: A synthesis. *Quaternary Geochronology*, 31, 119–154. Available from: <https://doi.org/10.1016/j.quageo.2015.09.006>
- Pope, R., Wilkinson, K., Skourtsos, E., Triantaphyllou, M. & Ferrier, G. (2008) Clarifying stages of alluvial fan evolution along the Sfakian piedmont, southern Crete: New evidence from analysis of post-incisive soils and OSL dating. *Geomorphology*, 94(1–2), 206–225. Available from: <https://doi.org/10.1016/j.geomorph.2007.05.007>
- Pope, R.J.J., Candy, I. & Skourtsos, E. (2016) A chronology of alluvial fan response to Late Quaternary sea level and climate change, Crete. *Quaternary Research*, 86(2), 170–183. Available from: <https://doi.org/10.1016/j.yqres.2016.06.003>
- Pope, R.J.J. & Wilkinson, K.N. (2005) Reconciling the roles of climate and tectonics in Late Quaternary fan development on the Spartan piedmont, Greece. *Geological Society Special Publication*, 251(1), 133–152. Available from: <https://doi.org/10.1144/GSL.SP.2005.251.01.10>
- Prager, C., Ivy-Ochs, S., Ostermann, M., Synal, H.-A. & Patzelt, G. (2009) Geology and radiometric ^{14}C -, ^{36}Cl - and Th-/U-dating of the Fernpass rockslide (Tyrol, Austria). *Geomorphology*, 103(1), 93–103. Available from: <https://doi.org/10.1016/j.geomorph.2007.10.018>
- Prescott, J.R. & Hutton, J.T. (1994) Cosmic ray contributions to dose rates for luminescence and ESR dating: Large depths and long-term time variations. *Radiation Measurements*, 23(2–3), 497–500. Available from: [https://doi.org/10.1016/1350-4487\(94\)90086-8](https://doi.org/10.1016/1350-4487(94)90086-8)
- Reilinger, R., McClusky, S., Paradissis, D., Ergintav, S. & Vernant, P. (2010) Geotectonic constraints on the tectonic evolution of the Aegean region and strain accumulation along the Hellenic subduction zone. *Tectonophysics*, 488(1–4), 22–30. Available from: <https://doi.org/10.1016/j.tecto.2009.05.027>
- Reilinger, R., McClusky, S., Vernant, P., Lawrence, S., Ergintav, S., Cakmak, R., Ozener, H., Kadirov, F., Guliev, I., Stepanyan, R., Nadariya, M., Hahubia, G., Mahmood, S., Sakr, K., ArRajehi, A., Paradissis, D., al-Aydrus, A., Prilepin, M., Guseva, T., Evren, E., Dmitrova, A., Filikov, S.V., Gomez, F., al-Ghazzi, R. & Karam, G. (2006) GPS constraints on continental deformation in the Africa–Arabia–Eurasia continental collision zone and implications for the dynamics of plate interactions. *Journal of Geophysical Research*, 111(B5), 26. Available from: <https://doi.org/10.1029/2005JB004051>
- Reimer, P. J., Austin, W. E. N., Bard, E., Bayliss, A., Blackwell, P. G., Bronk Ramsey, C., Butzin, M., Cheng, H., Edwards, R. L., Friedrich, M., Grootes, P. M., Guilderson, T. P., Hajdas, I., Heaton, T. J., Hogg, A. G., Hughen, K. A., Kromer, B., Manning, S. W., Muscheler, R., ... Talamo, S. (2020) The IntCal20 Northern Hemisphere Radiocarbon Age Calibration Curve (0–55 cal kBP). *Radiocarbon*, 62(4), 725–757. <https://doi.org/10.1017/rdc.2020.41>
- Rittenour, T.M., Goble, R.J. & Blum, M.D. (2003) An optical age chronology of Late Pleistocene fluvial deposits in the northern lower Mississippi valley. *Quaternary Science Reviews*, 22(10–13), 1105–1110. Available from: [https://doi.org/10.1016/S0277-3791\(03\)00041-6](https://doi.org/10.1016/S0277-3791(03)00041-6)
- Rittenour, T.M., Goble, R.J. & Blum, M.D. (2005) Development of an OSL chronology for Late Pleistocene channel belts in the lower Mississippi valley, USA. *Quaternary Science Reviews*, 24(23–24), 2539–2554. Available from: <https://doi.org/10.1016/J.QUASCREV.2005.03.011>
- Robertson, J., Meschis, M., Roberts, G.P., Ganas, A. & Gheorghiu, D.M. (2019) Temporally constant quaternary uplift rates and their relationship with extensional upper-plate faults in South Crete (Greece), constrained with ^{36}Cl cosmogenic exposure dating. *Tectonics*, 38(4), 1189–1222. Available from: <https://doi.org/10.1029/2018TC005410>
- Roda-Boluda, D.C., D'Arcy, M., Whittaker, A.C., Gheorghiu, D.M. & Rodés, Á. (2019) ^{10}Be erosion rates controlled by transient response to normal faulting through incision and landsliding. *Earth and Planetary Science Letters*, 507, 140–153. Available from: <https://doi.org/10.1016/j.epsl.2018.11.032>
- Rodés, Á., Pallàs, R., Braucher, R., Moreno, X., Masana, E. & Bourlés, L. (2011) Effect of density uncertainties in cosmogenic ^{10}Be depth-profiles: Dating a cemented Pleistocene alluvial fan (Carboneras fault, SE Iberia). *Quaternary Geochronology*, 6(2), 186–194. Available from: <https://doi.org/10.1016/j.quageo.2010.10.004>
- Rose, J., Meng, X. & Watson, C. (1999) Palaeoclimate and palaeoenvironmental responses in the western Mediterranean over the last 140 ka: Evidence from Mallorca, Spain. *Journal of the Geological Society*, 156(2), 435–448. Available from: <https://doi.org/10.1144/GSJGS.156.2.0435>
- Roucoux, K.H., Tzedakis, P.C., Lawson, I.T. & Margari, V. (2011) Vegetation history of the penultimate glacial period (marine isotope stage 6) at Ioannina, North-West Greece. *Journal of Quaternary Science*, 26(6), 616–626. Available from: <https://doi.org/10.1002/JQS.1483>
- Sadler, P.M. (1981) Sediment accumulation rates and the completeness of stratigraphic sections. *The Journal of Geology*, 89, 569–584. Available from: <https://doi.org/10.1086/628623>
- Savi, S., Norton, K.P., Picotti, V., Akçar, N., Delunel, R., Brardinoni, F., Kubik, P. & Schlunegger, F. (2014) Quantifying sediment supply at the end of the last glaciation: Dynamic reconstruction of an alpine debris-flow fan. *Geological Society of America Bulletin*, 126(5–6), 773–790. Available from: <https://doi.org/10.1130/B30849.1>
- Schaller, M., Blanckenburg, F., Veldkamp, A., Tebbens, L.A., Hovius, N. & Kubik, P.W. (2002) A 30 000 yr record of erosion rates from cosmogenic ^{10}Be in middle European river terraces. *Earth and Planetary Science Letters*, 204(1–2), 307–320. Available from: [https://doi.org/10.1016/S0012-821X\(02\)00951-2](https://doi.org/10.1016/S0012-821X(02)00951-2)
- Scherler, D., Bookhagen, B., Wulff, H., Preusser, F. & Strecker, M.R. (2015) Increased Late Pleistocene erosion rates during fluvial aggradation in the Garhwal Himalaya, northern India. *Earth and Planetary Science Letters*, 428, 255–266. Available from: <https://doi.org/10.1016/j.epsl.2015.06.034>
- Schildgen, T.F., Van Der Beek, P.A., Sinclair, H.D. & Thiede, R.C. (2018) Spatial correlation bias in late-Cenozoic erosion histories derived from thermochronology. *Nature*, 559(7712), 89–93. Available from: <https://doi.org/10.1038/s41586-018-0260-6>
- Shaw, B., Ambraseys, N.N., England, P.C., Floyd, M.A., Gorman, G.J., Higham, T.F.G., Jackson, J.A., Nocquet, J.M., Pain, C.C. & Piggott, M. D. (2008) Eastern Mediterranean tectonics and tsunami hazard inferred from the AD 365 earthquake. *Nature Geoscience*, 1(4), 268–276. Available from: <https://doi.org/10.1038/ngeo151>
- Shotton, F.W. (1972) An example of hard-water error in radiocarbon dating of vegetable matter. *Nature*, 240(5382), 460–461. Available from: <https://doi.org/10.1038/240460a0>
- Shuster, D.L., Ehlers, T.A., Rusmore, M.E. & Farley, K.A. (2005) Geology: Rapid glacial erosion at 1.8 ma revealed by $^4\text{He}/^3\text{He}$ thermochronometry. *Science*, 310(5754), 1668–1670. Available from: <https://doi.org/10.1126/science.1118519>
- Simpson, G. & Castelltort, S. (2012) Model shows that rivers transmit high-frequency climate cycles to the sedimentary record. *Geology*, 40(12), 1131–1134. Available from: <https://doi.org/10.1130/G33451.1>
- Stone, J.O. (2000) Air pressure and cosmogenic isotope production. *Journal of Geophysical Research - Solid Earth*, 105(B10), 23753–23759. Available from: <https://doi.org/10.1029/2000JB900181>
- Strasser, T.F., Runnels, C., Wegmann, K., Panagopoulou, E., McCoy, F., Digregorio, C., Karkanas, P. & Thompson, N. (2011) Dating Palaeolithic sites in southwestern Crete, Greece. *Journal of Quaternary Science*, 26(5), 553–560. Available from: <https://doi.org/10.1002/jqs.1482>
- Stuiver, M. & Polach, H.A. (1977) Discussion reporting of ^{14}C data. *Radiocarbon*, 19(3), 355–363. Available from: <https://doi.org/10.1017/S0033822200003672>

- Synal, H.-A., Stocker, M. & Suter, M. (2007) MICADAS: A new compact radiocarbon AMS system. *Nuclear Instruments and Methods in Physics Research, Section B: Beam Interactions with Materials and Atoms*, 259(1), 7–13. Available from: <https://doi.org/10.1016/j.nimb.2007.01.138>
- Tofelde, S., Schildgen, T.F., Savi, S., Pingel, H., Wickert, A.D., Bookhagen, B., Wittmann, H., Alonso, R.N., Cottle, J. & Strecker, M. R. (2017) 100 kyr fluvial cut-and-fill terrace cycles since the middle Pleistocene in the southern Central Andes, NW Argentina. *Earth and Planetary Science Letters*, 473, 141–153. Available from: <https://doi.org/10.1016/j.epsl.2017.06.001>
- Torres Acosta, V., Schildgen, T.F., Clarke, B.A., Scherler, D., Bookhagen, B., Wittmann, H., von Blanckenburg, F. & Strecker, M.R. (2015) Effect of vegetation cover on millennial-scale landscape denudation rates in East Africa. *Lithosphere*, 7(4), 408–420. Available from: <https://doi.org/10.1130/L402.1>
- Tucker, G.E. & Slingerland, R. (1997) Drainage basin responses to climate change. *Water Resources Research*, 33(8), 2031–2047. Available from: <https://doi.org/10.1029/97WR00409>
- Valla, P.G., van der Beek, P.A., Shuster, D.L., Braun, J., Herman, F., Tassan-Got, L. & Gautheron, C. (2012) Late Neogene exhumation and relief development of the Aar and Aiguilles Rouges massifs (Swiss Alps) from low-temperature thermochronology modeling and $^4\text{He}/^3\text{He}$ thermochronometry. *Journal of Geophysical Research - Earth Surface*, 117(F1), 1004. Available from: <https://doi.org/10.1029/2011JF002043>
- van Hinsbergen, D.J. & Meulenkamp, J.E. (2006) Neogene supra-detachment basin development on Crete (Greece) during exhumation of the South Aegean core complex. *Basin Research*, 18(1), 103–124. Available from: <https://doi.org/10.1111/j.1365-2117.2005.00282.x>
- Vernon, A.J., van der Beek, P.A., Sinclair, H.D. & Rahn, M.K. (2008) Increase in late Neogene denudation of the European Alps confirmed by analysis of a fission-track thermochronology database. *Earth and Planetary Science Letters*, 270(3–4), 316–329. Available from: <https://doi.org/10.1016/j.epsl.2008.03.053>
- Vockenhuber, C., Miltenberger, K.-U. & Synal, H.-A. (2019) ^{36}Cl measurements with a gas-filled magnet at 6 MV. *Nuclear Instruments and Methods in Physics Research, Section B: Beam Interactions with Materials and Atoms*, 455, 190–194. Available from: <https://doi.org/10.1016/j.nimb.2018.12.046>
- Waters, J.V., Jones, S.J. & Armstrong, H.A. (2010) Climatic controls on Late Pleistocene alluvial fans, Cyprus. *Geomorphology*, 115(3–4), 228–251. Available from: <https://doi.org/10.1016/j.geomorph.2009.09.002>
- Watkins, S.E., Whittaker, A.C., Bell, R.E., McNeill, L.C., Gawthorpe, R.L., Brooke, S.A.S. & Nixon, C.W. (2019) Are landscapes buffered to high-frequency climate change? A comparison of sediment fluxes and depositional volumes in the Corinth Rift, Central Greece, over the past 130 ky. *GSA Bulletin*, 131, 372–388. Available from: <https://doi.org/10.1130/B31953.1>
- Wegmann, K.W. & Pazzaglia, F.J. (2009) Late Quaternary fluvial terraces of the Romagna and Marche Apennines, Italy: Climatic, lithologic, and tectonic controls on terrace genesis in an active orogen. *Quaternary Science Reviews*, 28(1–2), 137–165. Available from: <https://doi.org/10.1016/j.quascirev.2008.10.006>
- Wickert, A.D. & Schildgen, T.F. (2019) Long-profile evolution of transport-limited gravel-bed rivers. *Earth Surface Dynamics (Pembroke, Ont.)*, 7(1), 17–43. Available from: <https://doi.org/10.5194/esurf-7-17-2019>
- Willenbring, J.K. & von Blanckenburg, F. (2010) Long-term stability of global erosion rates and weathering during late-Cenozoic cooling. *Nature*, 465(7295), 211–214. Available from: <https://doi.org/10.1038/nature09044>
- Wintle, A.G. & Murray, A.S. (2006) A review of quartz optically stimulated luminescence characteristics and their relevance in single-aliquot regeneration dating protocols. *Radiation Measurements*, 41(4), 369–391. Available from: <https://doi.org/10.1016/j.radmeas.2005.11.001>
- Wulf, S., Hardiman, M.J., Staff, R.A., Koutsodendris, A., Appelt, O., Blockley, S.P.E., Lowe, J.J., Manning, C.J., Ottoloni, L., Schmitt, A.K., Smith, V.C., Tomlinson, E.L., Vakhrameeva, P., Knipping, M., Kotthoff, U., Milner, A.M., Müller, U.C., Christanis, K., Kalaitzidis, S., Tzedakis, P.C., Schmiedl, G. & Pross, J. (2018) The marine isotope stage 1–5 cryptotephra record of Tenaghi Philippon, Greece: Towards a detailed tephrostratigraphic framework for the eastern Mediterranean region. *Quaternary Science Reviews*, 186, 236–262. Available from: <https://doi.org/10.1016/j.quascirev.2018.03.011>
- Zembo, I., Panzeri, L., Galli, A., Bersezio, R., Martini, M. & Sibilina, E. (2009) Quaternary evolution of the intermontane Val d'Agri Basin, southern Apennines. *Quaternary Research*, 72(3), 431–442. Available from: <https://doi.org/10.1016/j.yqres.2009.02.009>
- Zerathe, S., Braucher, R., Lebourg, T., Bourlés, D., Manetti, M. & Léanni, L. (2013) Dating chert (diagenetic silica) using in-situ produced ^{10}Be : Possible complications revealed through a comparison with ^{36}Cl applied to coexisting limestone. *Quaternary Geochronology*, 17, 81–93. Available from: <https://doi.org/10.1016/j.quageo.2013.01.003>

SUPPORTING INFORMATION

Additional supporting information can be found online in the Supporting Information section at the end of this article.

How to cite this article: Ott, R.F., Scherler, D., Wegmann, K.W., D'Arcy, M.K., Pope, R.J., Ivy-Ochs, S. et al. (2023) Paleo-denudation rates suggest variations in runoff drove aggradation during last glacial cycle, Crete, Greece. *Earth Surface Processes and Landforms*, 48(2), 386–405. Available from: <https://doi.org/10.1002/esp.5492>